Development of optical Sensors for Carbon Dioxide Detection

Nuno Alexandre Pereira Mendes
Master's in physics engineering
Department of physics and astronomy
2022

Supervisor
Luís Carlos Costa Coelho, Researcher, INESC TEC

Co-supervisor
Pedro Alberto da Silva Jorge, Assistant Professor, Faculdade de Ciências
Universidade do Porto

U.PORTO

FACULDADE DE CIÊNCIAS
UNIVERSIDADE DO PORTO

Todas as correções determinadas

pelo júri, e só essas, foram efetuadas.

O Presidente do Júri,

Porto, _____/_____/_____

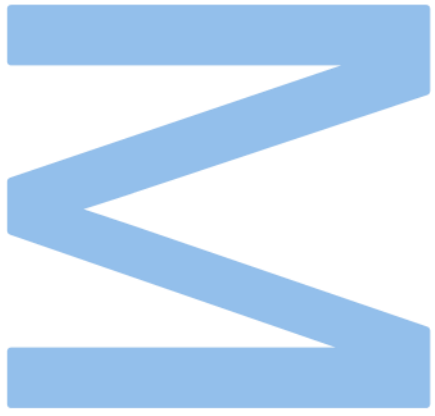

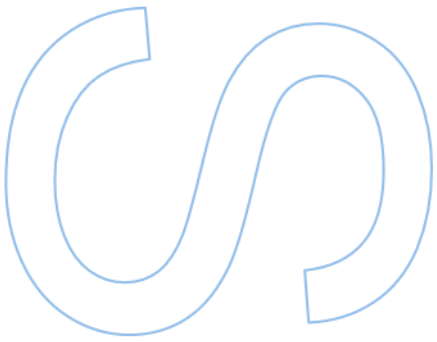

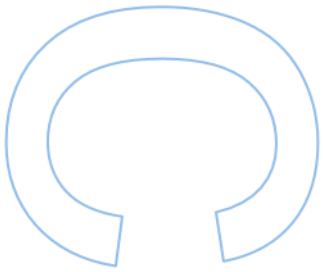

UNIVERSIDADE DO PORTO

MASTERS THESIS

Development of optical Sensors for Carbon Dioxide Detection

Author:
Nuno MENDES

Supervisor:
Luis COELHO

Co-supervisor:
Pedro JORGE

A thesis submitted in fulfilment of the requirements
for the degree of MSc. Engineering Physics

at the

Faculdade de Ciências da Universidade do Porto
Departamento de Física e Astronomia

November 25, 2022

Sworn Statement

I, Nuno Alexandre Pereira Mendes, enrolled in the Master Degree Engineering physics at the Faculty of Sciences of the University of Porto hereby declare, in accordance with the provisions of paragraph a) of Article 14 of the Code of Ethical Conduct of the University of Porto, that the content of this dissertation reflects perspectives, research work and my own interpretations at the time of its submission.

By submitting this dissertation, I also declare that it contains the results of my own research work and contributions that have not been previously submitted to this or any other institution.

I further declare that all references to other authors fully comply with the rules of attribution and are referenced in the text by citation and identified in the bibliographic references section. This dissertation does not include any content whose reproduction is protected by copyright laws.

I am aware that the practice of plagiarism and self-plagiarism constitute a form of academic offense.

_____

30/09/2022

Acknowledgments

I would like to thank the people that led me to this point in life.

First, to my mother and father, who's unconditional support helped me along my life.

My brother Tiago, who is the most reliable person I know with a vast knowledge in a great variety of fields.

I would like to acknowledge my advisor Luis Coelho, for his problem-solving skills, common sense, and levelheadedness. His supervision of the writing of this document was critical.

I would also like to thank my co advisor Pedro Jorge for his support of my work, which was indispensable.

To my colleague João Mendes, whose research was the base of the work that is here presented. His insight and knowledge helped this project move forward, his contributions to this work cannot be understated.

To my laboratory colleagues for their advice and guidance during my experimental work. Their expertise allowed for a great work environment, where a free flow of ideas was passed around and everyone helped each other.

To my host institution INESC TEC, for providing all the technical and scientific conditions for the completion of this project.

To Faculdade de Ciências da Universidade do Porto.

My good friend, Carlos who was there for me every step of the way.

To all my course colleagues, dedication, perseverance and good will helped me reach this point.

Resumo

Um tópico essencial ambos para o setor privado como para o setor publico é a monitorização de dióxido de carbono. Diversas indústrias como a indústria alimentar e a indústria de saúde necessitam de sensores de CO_2 por diversas razões. Um sensor colorimétrico de CO_2 foi desenvolvido com base num sensor previamente testado. O objetivo principal do sensor desenvolvido foi miniaturizar e compactar a versão testada anteriormente. Ambos os sensores usam um transdutor colorimétrico que muda de cor quando é exposto a CO_2. O objetivo destes sensores óticos é medir as diferenças de cor que originam de uma reação química entre o transdutor e o CO_2. Os dois sensores foram testados para CO_2 gasoso, e o sensor desenvolvido foi testado para CO_2 dissolvido. Foram obtidos resultados experimentais para CO_2 gasoso, onde um dos sensores foi caraterizado numa gama entre 1% e 3% CO_2 com um limite de deteção de 1.07% e um limite de quantificação 1.23%. O outro sensor foi caraterizado entre uma gama de 7% e 20 % CO_2 com um limite de deteção 1.87% e um limite de quantificação de 6.61%. O sensor desenvolvido mostrou potencial para medições para CO_2 dissolvido.

Abstract

An essential subject for both the public and business sectors is the monitoring of carbon dioxide. Many businesses, including the food industry and the health industry, require carbon dioxide sensors. A colorimetric CO_2 sensor was developed based on a previous tested Sensor. The main objective of the developed sensor was to miniaturize and compact the previous version. Both sensors make use of a colorimetric transducer, which changes color because of a chemical reaction when exposed to CO_2. To recognize and quantify the color changes in the transducer, an optical sensor was built. The two sensors were tested, for gaseous CO_2. One sensor was tested for dissolved CO_2. Experimental results were obtained for gaseous CO_2 were one of the sensors was characterized in a range between 1% and 3% CO_2 with a limit of detection of 1.07% and a limit of quantification of 1.23 %. The other sensor was characterized in a range between 7% and 20% CO_2 with a limit of detection of 1.87% and a limit of quantification of 6.61%. The developed sensor also showed promise for dissolved CO_2 measurements.

Key Words

Optical Sensor; CO_2 sensor; dissolved Carbon dioxide; optical fiber; colorimetric sensor;

Index of tables and figures

Abbreviations

N_2- Nitrogen

CO_2 – Carbon Dioxide

dCO_2 – dissolved Carbon dioxide

HCO_3^- - Bicarbonate Ion

H_2CO_3- Carbonic Acid

CO_3^{2-} - Carbonate Ion

GHG – Green House Gases

H_2O - Water

RAS – Recirculating Aquaculture System

MOS – Metal Oxide Sensor

ZnO – Zinc Oxide

SnO_2 – Stannic Oxide

TiO_2 – titanium dioxide

CeO_2 – Cerium Dioxide

Nb_2O_5 – Niobium oxide

OPAMP – Operational Amplifier

RGB – Red Green Blue

LOD – Limit of Detection

LOQ – Limit of Quantification

LED – Light Emitting Diode

TOA- tetraethylammonium hydroxide

pNPh- p-nitrophenol

NDIR – Non-Dispersive Infra-Red

Chapter 1 Introduction

1. Research Goals

Carbon dioxide (CO_2) monitoring is used in a variety of industries, and an endeavor sought by many governmental agencies. For industrial applications, CO_2 monitoring can vary from medical industry, food industry to aquaculture.

The main motivation for this thesis was to develop a new optical CO_2 sensor that can measure both dissolved and gaseous CO_2 and can be applied in a few industries.

The methodology was based on previous research, with the aim to miniaturize, compact a previously built sensor being developed around a colorimetric membrane whose fabrication process was optimized.

The main objective was to build sensors capable of being implemented for gaseous and dissolved CO_2 monitoring with high performance and providing a full characterization regarding its measurement range, limit of detection and limit of quantification.

1.1. Thesis Structure

This thesis is divided in 6 chapters, where CO_2 monitoring is contextualized, a colorimetric sensor is developed and tested.

The first chapter discusses the structure and motivation for this thesis.

The Second chapter provides an overview of CO_2 and its properties. The impact of high CO_2 levels on the environment are discussed. A few applications are discussed, along with the industry sectors where CO_2 sensor is required. Examples of CO_2 sensors are described together with their basic operations, unique advantages, and downsides.

The Third chapter describes the sensing methodology, including the colorimetric transducer, how it interacts with CO_2, how that reaction is converted into a color variation, and the gas system that was employed for measurements.

Fourth chapter presents the optoelectronic configuration in detail showing the design and implementation with a discussion about the main advantages.

The experimental findings using both sensors are displayed in the fifth chapter. This data concentrated on hysteresis effects, reversibility, and stability. For CO_2 gaseous concentrations, both sensors were calibrated. One of the sensors was tested for dissolved CO_2 but no calibration was performed.

The sixth chapter finishes with a characterization of each sensor for their respective range. Potential applications for each sensor, possible further improvements.

The research described in this thesis was given as an oral presentation at the 2022 European Optical Society Annual Meeting and as a poster at the Doctoral Congress in Engineering.

Chapter 2 Carbon Dioxide Properties and Sensing Methodologies

2. An overview

One of the most abundant gas on planet earth is CO_2, currently composing 0.04% of the atmosphere[1]. The control of atmospheric CO_2 is currently one of the main topics on the table of several governments and environmental associations [2]. Monitoring of CO_2 is increasingly a necessity, due to the increase of anthropogenic emissions[3]. Environmental concerns have been growing for the last 200 years, and anthropogenic CO_2 emissions have increased the atmospheric concentration from 280 parts per million(ppm) to 400 ppm[4]. Greenhouse Gases, acidification of oceans are all side effects of this phenomenon which has caught the attention of many agencies.

Gas sensors had a market size of roughly 823.1 million dollars in 2019[5], this means that gas sensors are sought after in both the private and public sectors. Many industries require accurate, small, and robust sensors for real-time monitoring in a range of applications. Sensors that can perform in extreme situations, such as high temperatures, high pressures, and high humidity, as well as other factors, are becoming increasingly important.

2.1. Carbon dioxide Properties

Carbon is the foundation of all life on Earth, the carbon atom has a valence of four electrons, which means it may create up to four bonds around itself. Forming these bonds is the most stable form an atom can take, as it fills its outer shell. This property is one of the reasons that makes it so abundant in life forms. Carbon dioxide is made up of a molecule containing two oxygen atoms joined by a covalent link to a carbon atom.

Because of its tendency to absorb infrared radiation, CO_2 is classified as a greenhouse gas with unpredictably harmful consequences on the ecosystem. Greenhouse gases have a negative impact on the environment in many nations. The impact of greenhouse gases on the environment drives the demand for carbon dioxide sensors. Monitoring atmospheric carbon dioxide is currently one of the key issues sought by many government and environmental agencies. Environmental concerns have been developing for the previous 200 years, and anthropogenic CO_2 emissions have increased the atmospheric concentration from 280 parts per million(ppm) to 400 ppm. Greenhouse Gases, acidification

of seas are all negative consequences of this phenomena which has drawn the attention of several agencies.

2.2. Carbon Dioxide measuring Applications

There is a great variety for uses of carbon dioxide sensors and the most common will be presented and discussed in this section

2.2.1.Ocean Acidification

Most life on Earth is dependent on the ocean, which covers the majority of the planet's surface. It is an important contributor to the world's biodiversity, and many biodomes rely on the ocean's stability to exist. In the last 200 years, since the beginning of the industrial revolution, the amount of carbon dioxide in the atmosphere has increased.

According to Henrys law, the amount of gas that is dissolved inside a liquid is proportional to the partial pressure above the liquid.

$$C = K_H P_a \tag{2.1}$$

Where C is the concentration of a gas, K_H is Henrys law constant and P_a is the partial pressure of the gas[6].

This suggests that the amount of dissolved carbon dioxide in the ocean rises proportionately to the atmosphere's carbon dioxide concentration. Which caused the pH of the surface seawater to decline by 0.1 units, that implies It resulted in a 30% spike in hydrogen ion concentration. This detail could have adverse effects on both the environment and the ecology and biodiversity.

Figure 1 shows the interaction between the increase of atmospheric CO_2, the rise in global temperatures, and how they bring harmful environments to living organisms.

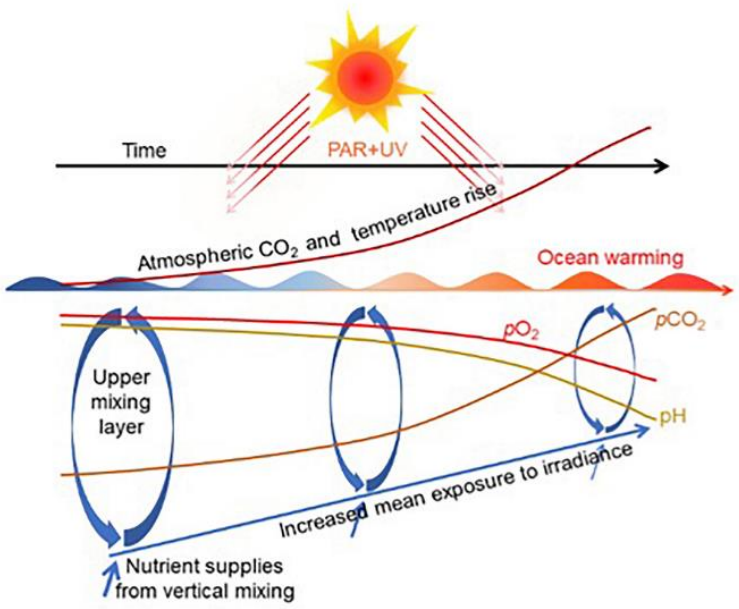

Figure 1: Ocean acidification, Ocean deoxygenation, and global warming all increase the amount of ultraviolet light that upper layer organisms are exposed to..[7]

Ocean Acidification describes the process by which the oceans become more acidic, and its pH is lowered. When CO_2 is dissolved in water, it tends to increase the concentration of hydrogen ions (H^+), which lowers the oceans pH. One of the main effects in sea life is that the hydrogen ions [H^+] react with carbonate ions [CO_3^{2-}] to form [HCO_3^-] [8], [9]. Marine organisms which form hard shells and skeletons by using calcium from the seawater are impacted by these changes, which makes it harder to access carbonate ions (Which bond with the excess hydrogen ions).This means that marine life forms such as corals, and mollusks can't form their shells naturally[10], [11]. The absence of coral reefs leads to a lack of coastal protection, that can have negative social and economic effects on the fishing and leisure industries. This equation shows how dissolved CO_2 forms carbonic acid and acidifies its environment. [9].

$$CO_2 + H_2O \leftrightarrow H_2CO_3 \leftrightarrow HCO_3^- + H^+ \leftrightarrow CO_3^{2-} + H^+ \qquad 2.2.$$

Reversing these oceanic changes will take a very long time[12].There is currently no known man-made solution that can stop ocean acidification during our lifetimes, and even if there were, it would only work locally and might have ramifications that are unpredictable. Reducing CO_2 emissions and maintaining an ecosystem that is stable enough to prevent biological impacts is the only viable way to stop polluting the oceans for a problem of this magnitude.

2.2.2.Food Storage & packaging

An ever-increasing food supply is desired in a consumer-driven economy [13]. Quality, quantity, and safety are now seen as being vital for consumers in the food industry, and many businesses strive to meet these high standards [12]. To prevent product damage, leakage, and spoiling, quality assurance mechanisms are required [14].

Bulk storage employs a controlled atmosphere where the air mixture is continuously and systematically maintained and monitored [14]. This method has been successfully employed to store grain, meat, fruit, and vegetables [15], [16]. The growth of insects, bugs, and fungi tends to cause deterioration during the storage of cereal grains and oilseeds. Heat, water, and carbon dioxide are produced in greater amounts when the grain begins to spoil. In most situations, the presence of high CO_2 concentrations (over 0.03 % compared to ambient), is considered as a signal of spoiling [17].

Carbon dioxide is an indicator for monitoring food quality and safety standards. In food packaging, the atmosphere inside the package is usually replaced for a certain mix of gases frequently made to slow down or stop metabolic activities preventing for example bacteria from growing and contaminating the food. Internal processes, including breathing, might take place during storage and alter the composition of the air[18].

Modified atmospheric packaging (MAP) is the name of this method, which is widely used in business [19]. Food packaging must have a way to keep food appetizing, aesthetically pleasing, and nutritive to attract customers. After being packed, fruits and vegetables continue to undergo metabolic processes that might lead to product degradation and microbial invasion [20]. By removing air from the packing and injecting a gas combination containing the necessary ingredients, this process is delayed. Some aerobic bacteria may have slower metabolic rates when food products like fruits and vegetables are kept in an environment with high CO_2 levels and low oxygen levels. Post-harvest impacts must be controlled, and CO_2 levels must be monitored [21].

Food shelf life is one of the key reasons for using this approach; it assesses how long a product will maintain qualities that are suitable for consumption after the packaging. Additionally, it guards against additional product deterioration that detracts from its appeal to customers, such discoloration and the formation of an unpleasant odor.

There are some variations of this method, where all the air is sucked out and the product is tightly wrapped around, this is called vacuum packaging.

Frequently in food packaging Nitrogen (N_2), and carbon dioxide are used. Nitrogen is utilized because it is an inert gas, whereas carbon dioxide is used to prevent the growth of aerobic microorganisms since oxygen is linked to oxidation processes and can induce this growth[21]. These gases should ensure that the atmosphere remains low in oxygen. Leaks may often be found by keeping food in an environment with high CO_2 levels inside the packaging. Monitoring the gaseous CO_2 concentrations allows for the early detection of leaks, protection of the food from air exposure, and prevention of deterioration.

In this industry gas concentrations for modified atmosphere packaging can vary from 3% CO_2 to 40% depending on the product that is being packaged.[16]

2.2.3.Capnography

Exhaled carbon dioxide is a residue that results from breathing's metabolic activities. When air is breathed in, oxygen (O_2) is transported and distributed into the bloodstream, where it reaches the cells. In the circulation, CO_2 is one of the metabolic byproducts of this exchange. The human body then exhales CO_2 as the result of this surplus being eliminated. It is commonly understood what makes up the human respiratory cycle. An average person breathes in 21 % oxygen, 0.04% carbon dioxide, and exhales 4 % CO_2 and 16% oxygen[22]. Capnography is the process of charting this cycle's partial pressure of CO_2 in the human breathing gases[23]. A non-invasive method of identifying a patient with lung problems, which leads to a reduction in airway complications.[24]–[26]

Exhaled gas is passed through a chamber where infra-red light absorption is seen, since CO_2 absorbs most strongly in the 4.26 micrometer wavelength, which is currently the case for most sensors used in this field[27]. The necessity for CO_2 sensors in the lower ranges is a result of these factors.

Figure 2 shows the typical capnography phases which is monitoring the human breath cycle for pCO_2. Phase 1 is the inhalation of CO_2 free gas, or dry air; phase 2 is the beginning of CO_2 exhalation from the lungs until it reaches a plateau. The third phase is the most significant it reveals if the lungs are to exhale a significant amount of air; End tidal CO_2 is the name of the pressure at the peak of this phase, which is used to prevent certain conditions including hypoxia and respiratory depression [27]. Phase 0 demonstrates that the breathed gas is devoid of CO_2.

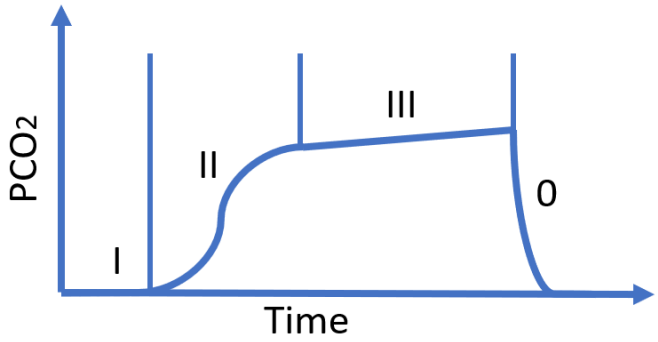

Figure 2: The typical capnography stages. (adapted from [28]).

The primary method for measuring CO_2 is infrared spectroscopy[27], and it can be seen from the carbon dioxide absorption spectrum that it has a significant absorption band around 4.26 micrometers in wavelength. As a result, the partial pressure of CO_2 in the exhaled breath may be calculated by a direct relationship between gas concentration and absorption bands. This indicates that the higher the concentration, the more infrared radiation is absorbed. The requirement to calibrate the sensor before each use is one of the numerous issues with this method, and the presence of water vapor can also alter measurements because it is a gas with a high infrared radiation absorption [29].

For capnography the required measuring range for a sensor is between 0.04% CO_2 and 4%[28].

2.2.4.Aquaculture

The controlled breeding, raising, and cultivation of aquatic lifeforms is known as aquaculture. It serves a variety of purposes, such as protecting threatened species, restoring habitats, and advancing business objectives. Safe habitats may be built in both freshwater and saltwater thanks to new technologies. The ocean is no longer able to meet the growing demand for fish food because of human activity.

Figure 3 it shows the growth of the aquaculture industry in 40 years, indicating a future need for dissolved CO_2 sensors.

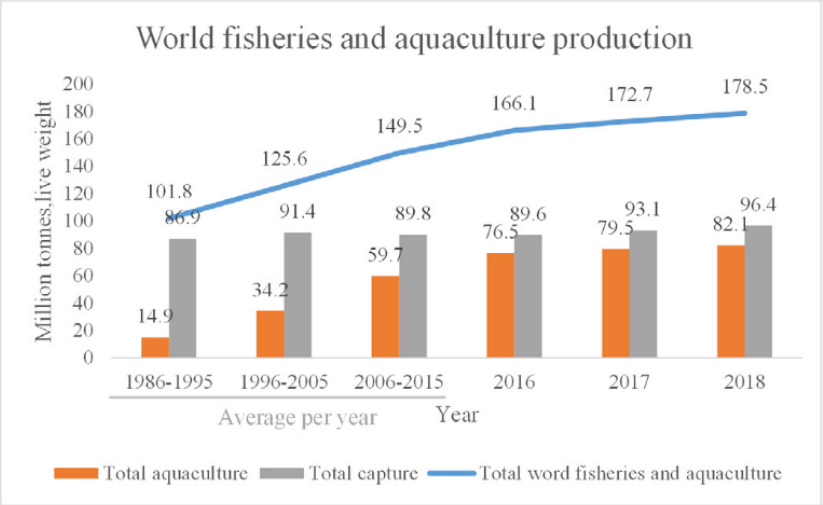

Figure 3: Aquaculture production from 1986 to 2018.[30]

Aquaculture has grown over the past few decades to suit consumer demand; by 2050, aquaculture will supply nearly all fish consumption in the food industry. Aquaculture is a key industry in the global food sectors, producing 80 million tons of fish food in 2016[31]. Fish raised in 37 different countries outnumbered fish harvested from the wild in the same year.

Recirculating aquaculture systems (RAS) is a technique that cleans and reuses water in a closed loop circulating system. When raising fish, this method is environmentally benign because no natural resources are used or squandered. Reusing the same water has led to an accumulation of metabolites that could endanger the health of the fish [32].

In aquaculture carbon dioxide is a naturally occurring residue, but exposure to high concentrations in water can cause health issues like an increased risk of nephrocalcinosis, stunted growth, and acidosis[32]–[34].

The relationship between size and growth in Atlantic salmon post-smolt farms is inversely correlated. Any extra 10 mg/L of dissolved CO_2 results in a growth decrease of 10% for these growth penalties, with a starting concentration of 12 mg/L. As a result, monitoring carbon dioxide is important in RAS[35].

For aquaculture, depending on the fish that are being farmed, dissolved CO_2 sensors are needed to monitor concentration levels between 5 mg/L and 40 mg/L [35].

2.3. Sensors for Carbon Dioxide Detection

A sensor is a device or system designed to record or measure a physical or chemical reaction. It converts an environmental change into a measurably clear signal.

A sensor may be broken down into 4 basic parts; First, a point of contact between the sensor and the environment; A transducer that transforms a physical change in the environment into a measurable signal, such as a rise in voltage, for example. The converted signal's processing, amplification, and measuring components that transform the signal into a read[36].

The transducer, which is typically a sensor's most basic element and the source of its restrictions, serves as the foundation for the remainder of the sensor, which is constructed around it[37].

To evaluate the performance of a sensor response time, selectivity, sensitivity, range, reversibility, and recovery time as well as the cost of fabrication and the stability of the signals are all important parameters. Range shows, the interval of concentrations that each sensor is calibrated to measure. Response time measures the time interval between the sensor receiving its target gas and the corresponding signal. Selectivity measures if other gases affect the measuring signal. Reversibility compares if the sequential of the same gas concentration measurements can measure the same signal meaning it says if the sensor can recover its original signal. Sensitivity measures the minimal input for sensor output to change, which in this case is the smallest amount of the target gas that can be present.

For carbon dioxide measuring a few types of sensors are used in the market, there are dry and wet sensors that measure either gaseous or dissolved carbon dioxide. The main difference between these sensors is the environments for which they thrive. In the next subsection the types of sensor used on the market are discussed.

2.3.1. Types of CO_2 sensor on the market

A general comprehension of the types of sensors offered on the market is necessary to comprehend the advantages and disadvantages of each type of sensor. A brief analysis of the types of sensors used for CO_2 is discussed in this subchapter.

2.3.2.Metal Oxide Sensors

Metal oxide sensors (MOS) are solid state sensors that vary in conductance when exposed to their target gas. Usually, they fall into two categories, where the sensor is characterized either by surface conductance effects or by bulk conductance effects. The operating method depends on the temperatures, where surface conductance works between 400 to 600 Celsius and the bulk conductance works above 700. At low temperatures, materials like SnO_2 and ZnO are used for surface conductance, whereas TiO_2, CeO_2, and Nb_2O_5 are employed for bulk conductance at high temperatures.[38], [39] A heater is a necessity to operate these sensors, which tend to have high power consumption.[40]

Before beginning direct measurements, the sensor surface is heated to high temperatures [41]. After heating, the sensor material's surface absorbs oxygen from the air around it. These oxygen particles interact with the sensor's surface material, increasing the sensor's resistance in n-type materials while decreasing it in p-type ones. When these sensors are exposed to the target gas, in this example, CO_2, they wish to measure the concentration of, the adsorbed oxygen goes through an oxidation-reduction reaction that changes the material's electrical resistance or the target gas can react directly with the oxide from the surface material[42]. Figure 4 depicts the behavior of the sensor's surface in relation to the target gas it is trying to measure as well as how the resistance values vary based on the type of materials used.

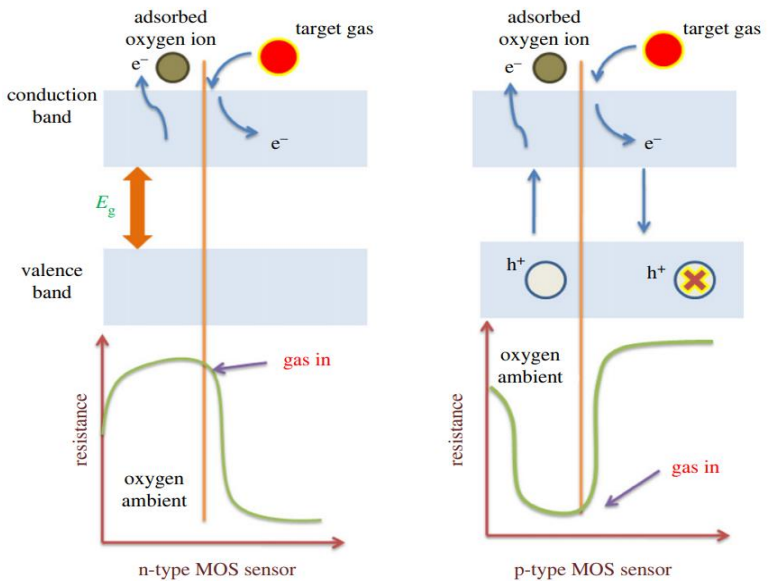

Figure 4: Interaction between MOS sensors, oxygen and their target gas.[42]

A reference conductivity is calculated based on the sensor’s interactions with oxygen where:

$$\sigma = A * exp\left(-\frac{E_A}{K * T}\right) p_O^{\frac{1}{N}} \quad 2.3$$

Where σ is the electrical conductivity, A is a constant, E_a is an activation energy, T is the temperature, K is an equilibrium constant and N is a bulk defects constant.

In n type sensor the response is defined by the following equation[42]:

$$S = \frac{R_g}{R_a} \quad 2.4$$

While for p type MOS sensors the response is defined by the following equation[42]:

$$S = \frac{R_a}{R_g} \quad 2.5$$

In these equations R_a is the resistance of the sensor in the presence of dry gas and R_g is the resistance of the sensors in the presence of the target gas.

2.3.3. Electrochemical CO_2 sensors

In electrochemical sensors a chemical reaction occurs between the target gas and the sensor where an electrode is used has a transducer to convert this reaction into an electrical signal. For carbon dioxide sensors type III potentiometric sensors measures the potential difference between a working electrode and a reference electrode to determine the gas concentration.

The Severing Haus-type sensor consists of a pH sensitive glass electrode that is covered by a bicarbonate solution where a chemical reaction occurs in the presence of carbon dioxide. The solution is enveloped by a hydrophobic gas permeable membrane, which protects the sensor from water and other electrolytes and allows for the measuring of dissolved and gaseous carbon dioxide. A reference electrode is used to compare to the sensing electrode [43].

A typical Severing Haus sensor is shown in Figure 5, where CO_2 diffuses into an electrolyte through a gas permeable membrane, combining with the electrolyte to raise its pH.

The glass electrode and the reference electrode take these reactions and turn them into an electrical signal.

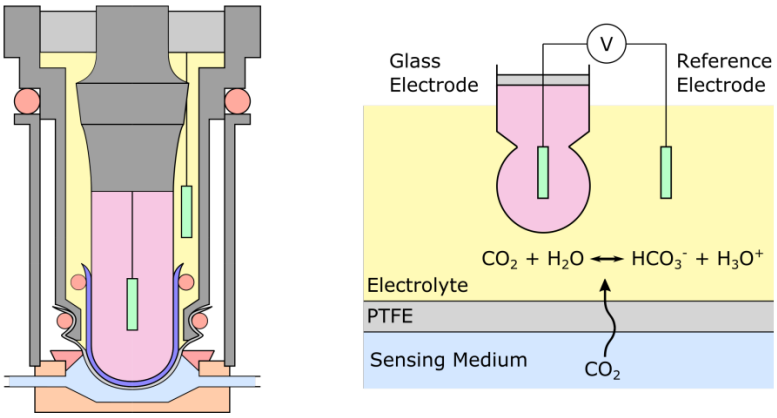

Figure 5: A simplified schematic of the Severinghaus sensor (on the right) and the sensor in its original configuration (on the left).. [44]

The electrical signal can be described by the Nernst type equation[45]:

$$E = k - \left(\frac{RT}{zF}\right) ln(Q) \qquad 2.6$$

Where R is a universal gas constant, T is the temperature, F is the faraday constant, z is the charge involved in the reaction, Q is the reaction quotient.

2.4. Optical CO_2 Sensors

In optical sensors, electromagnetic radiation interactions with either solid or liquid substances are utilized to analyze chemical interactions. Both infrared and visible light as well as ultraviolet radiation can be used for this purpose.

The feature that sets optical sensors apart from other types of sensors is capability to employ optical changes as a measuring tool for measurements. It allows optical sensors to determine a target's concentration by correlating optical properties.

According to the IUPAC classification optical sensors can be subdivided by the optical properties they measure, which can be by absorbance, luminescence, reflectance, refractive index, etc.[46]

Absorbance is measured in transparent mediums where, the analyte absorbs light in a specific light wavelength, reflectance measures the light that is reflected back by a non-transparent media, luminescence is the measurement of an emission of light due to a chemical reaction and changes in the refractive index of the medium that light transverses[46].

The capability to incorporate these sensors to measure almost any physical and chemical parameters is highly sought after. Fiber optical sensors are highly desirable due to their immunity to electro-magnetic and radio interference and long-range abilities to maintain information.

2.4.1.Nondispersive Infrared Sensor

Nondispersive infrared (NDIR) sensors are a type of sensors used to measure gas concentrations, through a spectral analysis. The method of measuring carbon dioxide using NDIR sensors is based on the correlation between concentration of a gas and its absorption of electromagnetic radiation [47]. A gaseous substance's concentration may be determined if its absorption spectrum is known, by using the Beer-Lambert law, there is a way to correlate this absorption with the gas concentration[47].

In NDIR sensors, an infrared light source is employed, and the sample is injected into a gas chamber. A wavelength filter made specifically for the target gas is placed in front of an infrared light detector.

A comparison between the target gas chamber's measured signal and the reference signal produces an absorption signal.

An illustration of an NDIR sensor is shown in Figure 6, where to measure the gas concentration, an infrared lamp sends a light signal through a sampling tube. Two thermopiles then receive the light signal, one as a reference signal and the other as the measured signal, to produce an absorption signal.

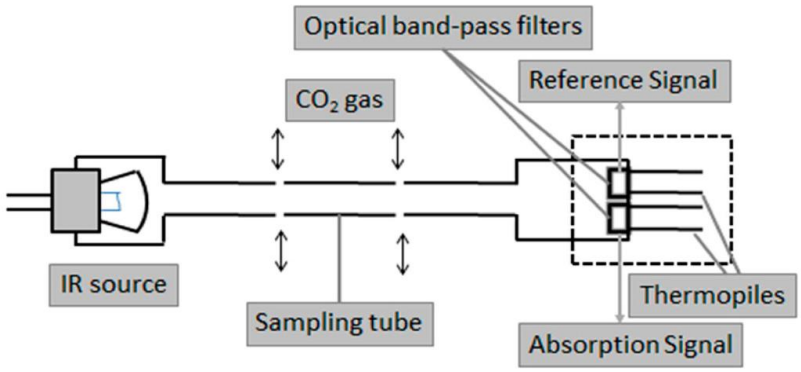

Figure 6: Structure of an NDIR sensor.[48]

Carbon dioxide has a well-established and characterized light absorption in the wavelength range of 4.26 micrometers[49]. This indicates that the more infrared light is absorbed, the

higher the concentration of CO_2. Based on this fact, a connection between gas concentrations and absorption bands may be constructed. As a result, it is also possible to determine the amounts of other gases in an environment that has been well monitored.

A change in absorbance is utilized as a measurement instrument for NDIR sensors. The relationship between light attenuation and the characteristics of the medium through which light is being transmitted is explained by the Beer-Lambert law. The relationship between the light that is transmitted through a substance and the light that was first emitted is known as transmittance and is explained by the following equations[50].

$$T = \frac{I}{I_0} \tag{2.7}$$

Where I is the transmitted light, and I_0 is the emitted light. While absorption is the logarithmic relationship with transmittance[50].

$$Absorbance = -log(T) \tag{2.8}$$

Absorbance shows how much of the emitted light is attenuated when it is transmitted through material.

The Beer-Lambert law is a combination of two laws[50], [51],one states that there is a direct correlation between the absorption of light going through a material and its length, that is explained in the following equation:

$$A \; \alpha \; l \tag{2.9}$$

And a second law that states that there is a direct correlation between absorption and gas concentration.

$$A \; \alpha \; c \tag{2.10}$$

In its most modern form, this law adds a constant that reflects the molar absorption coefficient.

$$A = \epsilon l c \tag{2.11}$$

Where ϵ is the Molar absorption coefficient, l is the optical path length that the light transverses the medium and c is the Molar concentration of the target gas.

This means that a change in light absorption of a specific light wavelength is correlated with the concentration of carbon dioxide.

Figure 7 demonstrates a high peak in infrared light absorption at around a 4.26 μm wavelength, which is the underlying principle for all NDIR sensors.

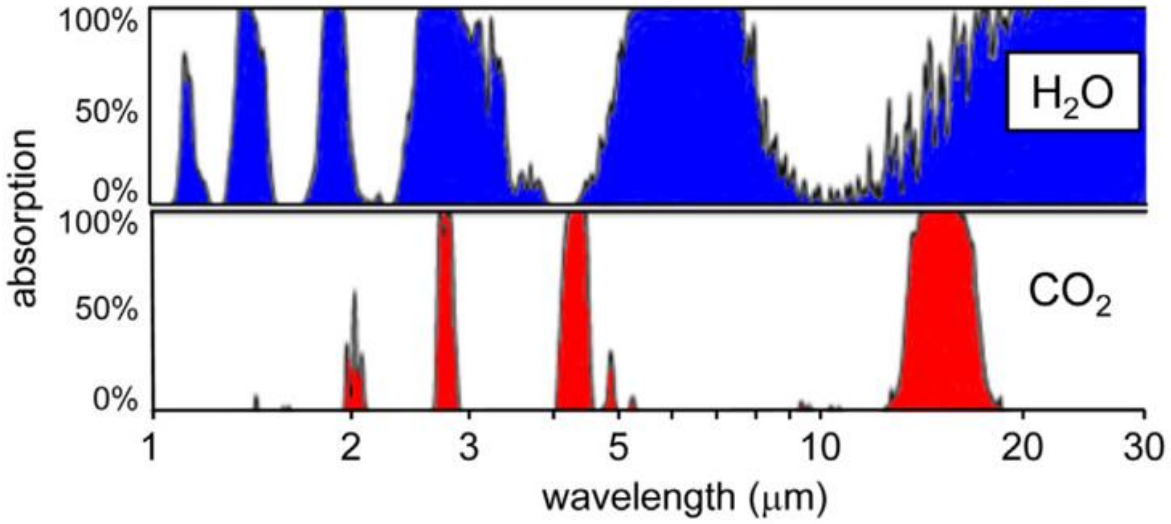

Figure 7:Atmospheric Absorption spectrum of the two biggest greenhouse gases, including CO_2 [52]

This kind of sensors tend to be affected by temperature changes, water vapor and atmospheric pressure. NDIR sensors are used to measure atmospheric concentration of carbon dioxide and for capnography.

2.4.2.Colorimetric pH sensors

When exposed to CO_2, colorimetric sensors change color, which is subsequently translated into an electrical signal. These sensors have the highest levels of selectivity and specificity. To analyze color changes, spectrometers—which are typically bulky and not practical — are widely utilized for a very thorough spectrum study. Typically, photodiodes and light filters with extremely narrow wavelength ranges are being applied to the miniaturization of sensors[53].

These kind of sensors usually uses a pH-sensitive dyes that, which in the presence of CO_2, tend to change color due to a chemical reaction with CO_2 that changes its internal pH[54], [55].

$$CO_2(g) \rightleftharpoons CO_2(aq) \quad 2.12$$

$$CO_2(aq) + H_2O \rightleftharpoons H_2CO_3 \quad 2.13$$

$$H_2CO_3 \rightleftharpoons H^+ + HCO_3^- \quad 2.14$$

Usually the pH sensitive dye (HD) is dissolved either in its anionic (D^-) or protonated (HD) form.[46]

$$HD \rightleftharpoons H^+ + D^- \quad 2.15$$

They typically consist of a colorimetric pH-sensitive dye (HD), a quaternary ammonium hydroxide(Q^+) that serves as an ion-paring agent, used to solubilize the dye, and a gas permeable membrane that allows the passage of CO_2 but not water since water might harm the dye's internal chemistry.

$$Q^+D^-.xH_2O + CO_2 \rightleftharpoons Q^+HCO_3^-.(x-1)H_2O.HD \quad 2.16$$

For wet sensors, CO_2 diffuses through a gas permeable membrane, a chemical reaction occurs with the pH sensitive dye and an equilibrium is achieved which is then measured, while in dry sensors the gas permeable membrane is sometimes used as protection.

Table 1: Different types of sensors, advantages and disadvantages.(Adapted from [37])

Type of sensor	Measured Quantities	Principle	Advantages	Disadvantages
MOS based Sensor	Conductivity	Conductometric	Fast response time, low cost, long life time. Wide range of target gases.	High-Energy Consumption, sensitivity to environmental factors.
Electrochemical Sensor	voltage	Potentiometric.	Can measure toxic gases in low concentration	Sensitivity to environmental factors
Optical Sensor	Light intensity, wavelength, refractive index	Absorbance, reflectance, fluorescence	High Sensitivity Immunity to electro magnetic interference	High cost and difficulty in miniaturization

Chapter 3 Methodology and Chemistry

The basis of the optical system and the chemical/colorimetric modifications brought on by CO_2 absorption in the colorimetric membrane are both detailed in this chapter. The colorimetric technique, which was based on previous research and was used for all measurements, is described. A thorough explanation of the colorimetric membrane's fabrication and encapsulation, as well as the gas testing system, are presented.

3. Methodology

A chemical membrane based on colorimetry was developed to be sensitive to Carbon dioxide and a full optoelectronic system was built to detect small color changes with the highest resolution possible.

The following block diagram of figure 8 explains the primary methodology underlying colorimetric-based sensors.

Figure 8: block Diagram of a typical colorimetric sensor.

A light source that transmits light via a colorimetric membrane makes up the sensor architecture. An optical signal from this membrane is then captured, processed, and a CO_2 measurement is acquired.

Since this sort of sensor is modular, it may be modified with alternative components that use the same basic operating principles for each element in the block diagram.

The basic components for a colorimetric sensor are shown in figure 9.

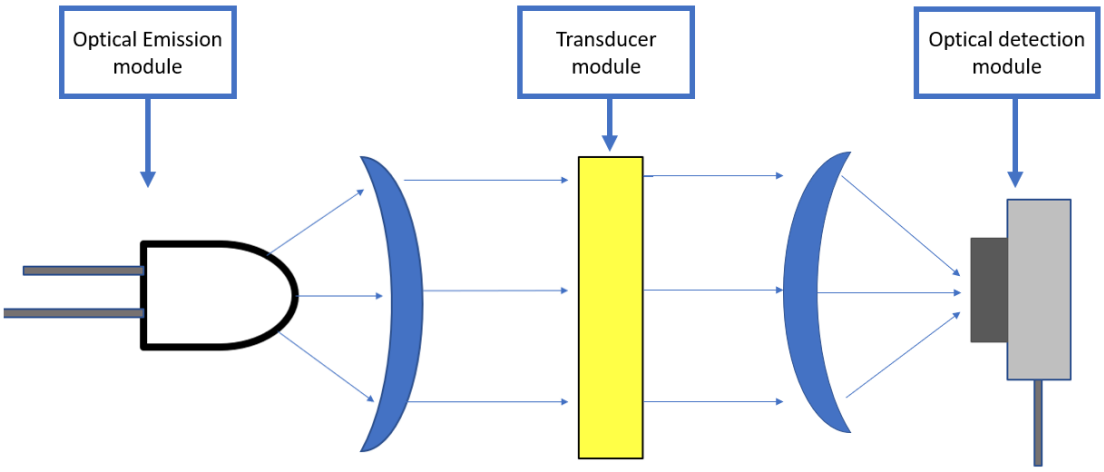

Figure 9: A light source, a transducer, and a signal capture are shown in this diagram to show how the created sensor is configured.

An optical emission module, which in this instance can be any type of light source in the transducer absorption spectrum, is shown on the left side of the picture. A transducer module in the center transforms a CO_2 interaction into a colorimetric effect. An optical signal is detected and processed for measurements by an optical detection module on the right side.

This sort of work was based on earlier research [56], [57], but for the objectives of optimization and downsizing, a novel configuration was constructed in this thesis.

3.1. Colorimetric Cocktail

For the fabrication of the chemical membrane the following chemical reagents were used; p-nitrophenol (pNPh) (Sigma-Aldrich ReagentPlus,>995), tetraethylammonium hydroxide solution(TOA-OH;20% in methanol, Sigma Aldrich) was used as a quaternary ammonium (TOA-OH), Hydrogel D4 (AdvanceSource Biochemicals, 10% in Ethanol, 96%; Lawrenceville, NJ, USA) was used as a polymer to produce a homogeneous membrane and Sylgard 184 (Dow Corning, 10:1, Midland, MI, USA) was used to encapsulate and protect the chemical membrane.

For the preparation of the chemical cocktail, 5 mg of p-nitrophenol (pNPh) was dissolved in 0.05 ml of MeOH:H_2O solution, which was mixed for 15 minutes using a magnetic stirrer. After mixture, an additional 0.5 ml of 0.5M TOA-OH was added, which was stirred again. After the pNPh dissolves completely, 0.1 ml of a Hydrogel solution was added (10% in ethanol, 96%), which was then stirred for another 15 minutes.

The final cocktail was then spread on a mylar foil by spin coating (900 rpm for 60 seconds), and left to dry for about 2 hours, which then is stored inside a fridge prior to use.

3.1.1. Chemical Membrane Chemistry

A dry optical carbon dioxide sensor can be broken down into a few basic components: a pH-sensitive dye, a phase transfer agent that dissolves the anionic form of the pH-sensitive dye, a hydrophilic polymer, and a gas permeable membrane to cover the exposed sensing layer.

A chemical equilibrium is created between the anionic and cationic versions of the phase transfer agent and the pH-sensitive dye because of the phase transfer agent's reaction with the sensing dye.

These sensors work primarily on the principle that CO_2 diffuses through a gas permeable membrane and interacts with the pH sensitive dye.

The following equation may be used to describe the colorimetric response in conventional colorimetric CO_2 sensors where a pH-sensitive dye is chemically reacting and changing its color. (Adapted from[58]).

$$D^-(Color\ A) + H^+ \leftrightarrows DH\ (Color\ B) \quad 3.1$$

Where color A represents the color of the deprotonated dye, while the color B is the protonated dye.

The colorimetric intensity of the pH-sensitive dye serves as the basis for CO_2 monitoring. The general chemical mechanism comes from an association with a few water molecules, which is described by the following equation[59]:

$$Q^+\ D^-.\chi H_2O + CO_2 \leftrightarrows\ Q^+HCO_3^-.(\chi - 1)H_2O.HD \quad 3.2$$

Where $Q^+\ D^-.\chi H_2O$ represent the deprotonated pH sensitive dye. This procedure involves reversibly protonating the pH-sensitive dye such that it will produce $Q^+HCO_3^-.(\chi - 1)H_2O.HD$ when exposed to CO_2.

Following the equations above, the sensor works by using an ion pair formation, where a pH sensitive dye (formed by the pNPh) in its deprotonated anionic form, interacts with the quaternary ammonium (TOA^+) forming the ion pair ($TOA^+\ pNPh^-$). Carbon dioxide sensing comes from an association with a few water molecules ($TOA^+\ pNPh^-.\chi H_2O$), produced by air humidity.

$$TOA^+\ pNPh^-.\chi H_2O + CO_2 \leftrightarrows\ TOA^+HCO_3^-.(\chi - 1)H_2O.HpNPh \quad 3.3$$

The membrane's internal pH balance is affected by a chemical interaction with CO_2, which acidifies the membrane directly. The internal pH levels of the membrane are associated with the color of the membrane.

A sensing membrane with a yellow color means that there is a stronger absorbance in the blue light spectrum. As the sensing membrane reacts with CO_2, its color will change, meaning that its absorption spectrum changes when exposed to different CO_2 concentrations. An absorption based optical system was built to measure these small color variations. All further measurements that are presented come with these principals in mind.

3.1.2. Encapsulation of the Colorimetric Membrane

The sensing membrane was enclosed with a silicone elastomer, Sylgard 184, which comes in two parts, a base and a curing agent that are mixed with each other in a 10:1 ratio, respectively. During the mixing process, air bubbles tend to form inside the mixed solution; since Sylgard cannot cure with air bubbles inside the mixture, they are removed by using a vacuum pump. Figure 10 shows the pieces used for encapsulating membranes.

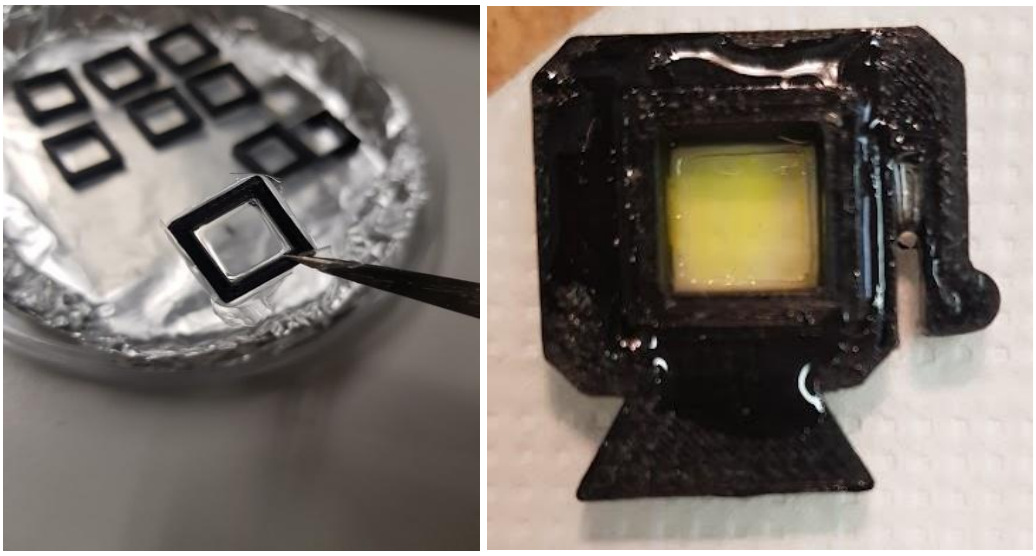

(a) (b)

Figure 10: a) A 3D printed piece is covered with Sylgard 184 to encapsulated the colorimetric membrane. b) With the Sylgard membrane coating the sensor surface, a chemical sensing membrane is put into the 3D manufactured Supports.

Using a spinner, a thin coating of Sylgard 184 was applied to a substrate (Mylar foil), and 3D printed components were then attached to this layer while it cured. The supports were then attached with the sensing membrane after the thin coating of Sylgard 184 had formed and adhered to them.

The use of an elastomer provides protection to the sensing membrane from unwanted material, like dust particles. Because of its elastic mechanical properties and chemical inertness, the coating is ideal for encapsulation. Sylgard 184 is colorless so it's ideal for colorimetric measurements. Support components were created to align the membrane in relation to the Sylgard-covered piece, the light source, and the detector.

The slits in each support piece were filled with Araldite, an epoxy glue made by mixing resin with a hardening agent to create a solid structure that is both chemically (can't be dissolved by most solvents) and thermally resistant (operates between -30ºC and 65ºC).

3.1.3. Colorimetric Behavior

In order to examine how variations in color occur in response to CO_2 exposure, the absorption spectra of the colorimetric transducer were measured using a spectrometer, a white light source, and a chemical membrane. To obtain color variations, three concentrations were selected, 0% CO_2, 50% CO_2, and 100% CO_2.

In figure 11, the absorption spectrum for the same membrane was measured for different concentrations. Using a spotless mylar foil surface and white light transmission, a reference signal was produced.

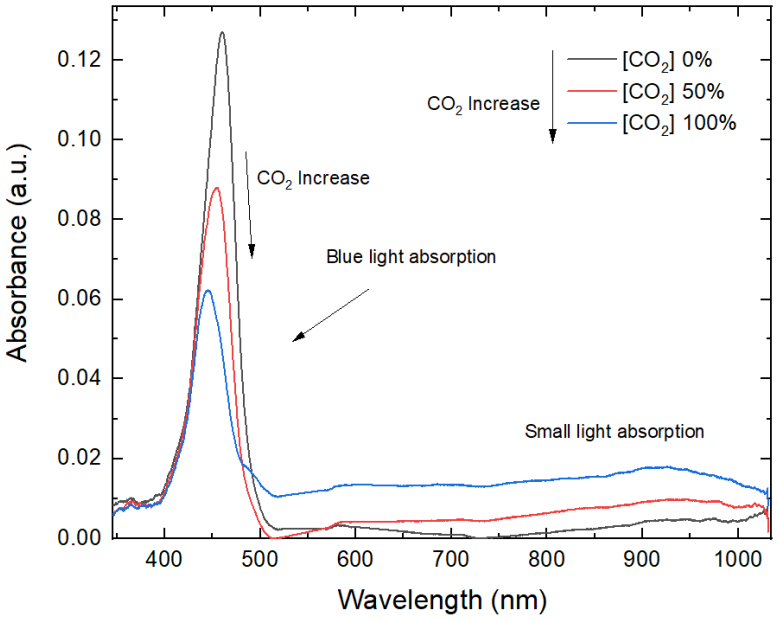

Figure 11: Absorption spectrum of the sensing membrane, using white light as a source.

A clear absorption band is observed around 470 nm, which corresponds to blue light. The graphic shows that the absorption value drops, as the amount of carbon dioxide increases, meaning that more light goes through the sensing membrane as CO_2 exposure increases.

Figure 12 shows two light signals: a red signal that is unaffected by CO_2 levels and a blue signal whose amplitude varies with exposure. Two signals are used to make certain that any change in amplitude is due to the colorimetric transducer and not changes in the overall signal. The image depicts six overlapping spectra, each of which represents a level, where a rise in the blue signal indicates that the CO_2 level has increased but, in each spectrum, the red signal mostly remains unchanged.

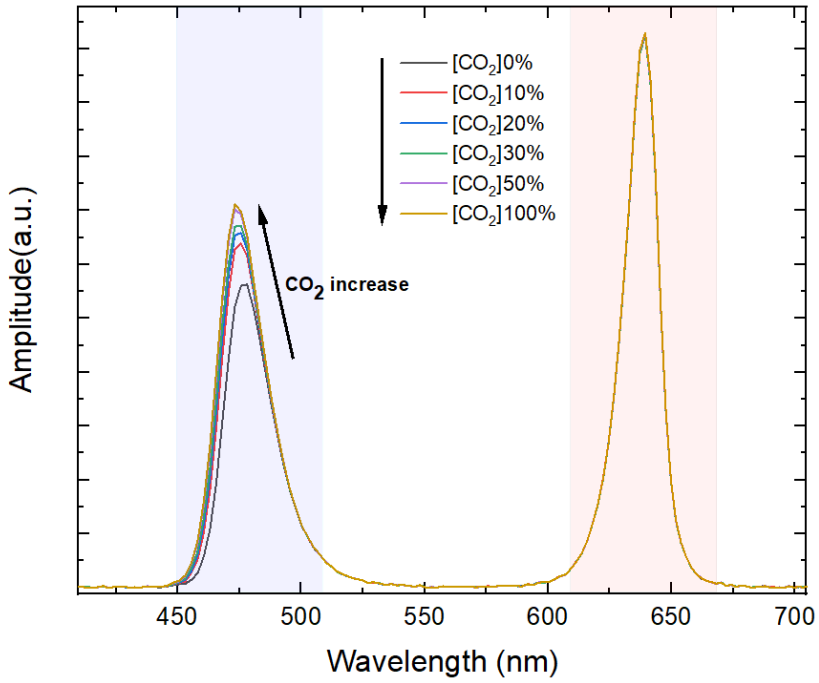

Figure 12: A Transmission spectrum of the sensing membrane.

The main objective is to correlate color changes for various CO_2 concentrations with optical signal amplitudes by creating amplitude/CO_2 concentration correlations.

3.2. Experimental setup

A gas system was created to produce different gas concentrations in order to evaluate the sensors' capacities and characteristics. This section provides a thorough explanation of this system.

3.2.1. Gas System

To test CO_2 sensors for gaseous concentration, a gas system was constructed. The system operates by injecting controlled amounts of gas, in this case a mixture of nitrogen (N_2) and CO_2. The gas mixture injected was controlled by mass flow controllers (Brooks, SLA5800 series; Hatfield, PA, USA). A gas mixing vessel that held water to humidify the air and guarantee a homogeneous mixture was used for each gas injection. A flow rate of 500 ml/min was maintained throughout measurements. Next the gas was sent inside a measurement chamber where the sensor was placed for testing. Injections of N_2 were employed to drive out or purge the gas inside the measuring chamber since it is non-reactive/Inert and ideal for purging gasses.

Figure 13 shows the whole gas system, including the sensor.

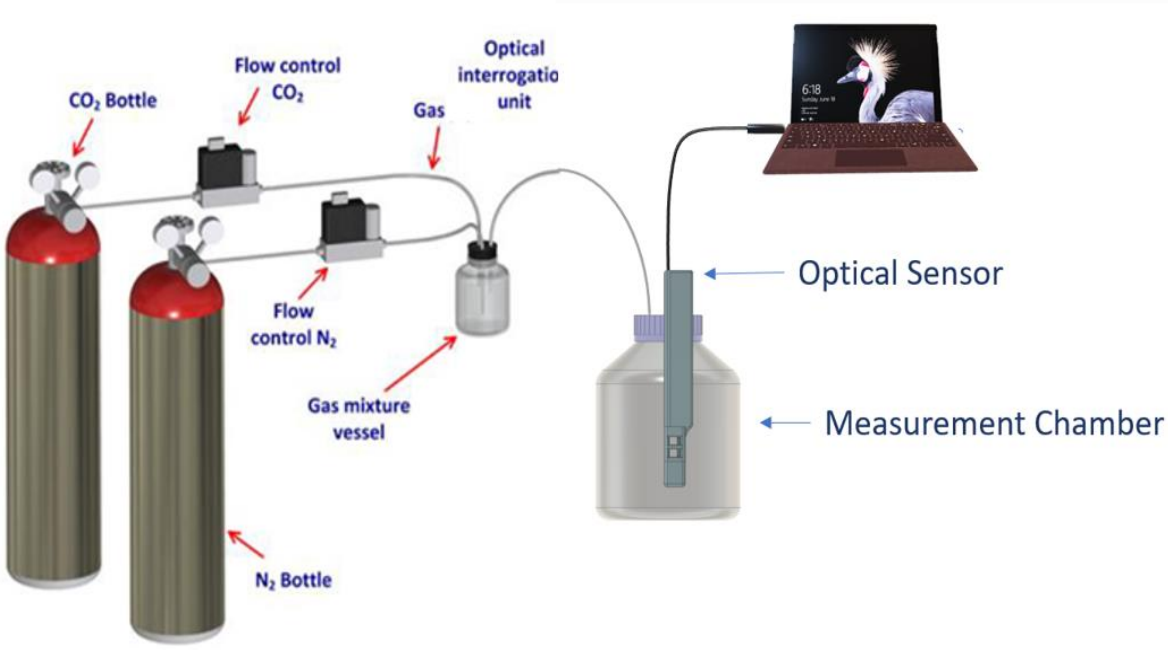

Figure 13: Gas system setup for testing purposes(Adapted from [56]).

The primary idea behind this technique is that the previous gas concentration will be flushed out by the fresh one that is being introduced into the measuring chamber. Since its possible to observe the sensors' responses between concentrations, this kind of arrangement is perfect for calibrating sensors.

The downside of this system is that any response time the sensor gives, must take into account the amount of time that takes for the gas to be flushed out. This means this system is not adequate to measure the effective response time of the chemical membrane.

3.3. Dissolved Gas System

A similar system was used to measure dissolved CO_2 concentrations. The Sylgard 184 elastomer is porous which means the CO_2 molecules can pass through and reach the chemical surface, but the water molecules can't, which makes the membrane impermeable to water.

This makes the transducer work in both an aqueous environment and a gaseous environment, meaning it's a dry and wet sensor. The main gas system was kept in the same configuration as in the previous subchapter. The main change was the addition of water to the measurement chamber during testing, which submerged the sensor. Due to the encapsulation by an elastomer, the sensing membrane was shielded from water damage. Figure 14 shows, Gas injections were employed to regulate the amounts of dissolved CO_2 inside the measuring chamber.

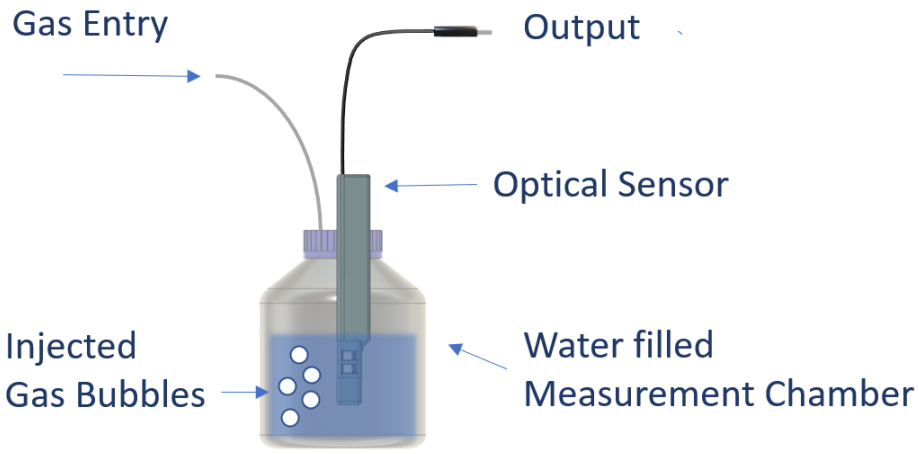

Figure 14: Dissolved Gas system setup for testing purposes.

One of the primary differences between the first set of data and the second is that the measuring chamber included 50 ml of deionized water. The quantity of water utilized was used to shorten the time between injecting gas and the CO_2 dissolving in the water. Dissolved CO_2 measurements take longer than measurements of gaseous CO_2 because the injected gas bubbles need to dissolve in the deionized water.

Chapter 4 Sensor Development and Design

4. Development of Sensors

This chapter provides a thorough explanation of how the electronics that make up the whole system were developed. The sensor encasing construction and how each component fits within are displayed. The communication between the computer and microcontroller of the embedded system is described.

The goal of the two sensors, which were both developed using a colorimetric membrane, is to measure and quantify color changes. The primary distinction between them is that Sensor A employs fiber optics to capture the light signal and a spectrometer, whereas Sensor B transforms an optical signal into an electrical signal before processing it.

4.1. Sensor A

A sensor was previously designed for measurements in both gaseous and aqueous environment[56]. In this prototype a transmission setup was designed, where the sensing layer is placed between an RGB LED (KingBright Europe, Germany), and a large core optical fiber(Thorlabs, FT600UMT, USA) that is connected to a spectrometer (Hamamatsu C12880MA, Japan), used for transmission spectral analysis of the sensing membrane. For Sensor A, a version of the transducer that was more sensitive to pH changes and therefore more sensitive to CO_2 was used. This was developed for aquaculture purposes, and the main difference is in the colorimetric cocktail which used poly-p-nitrophenol, instead of p nitrophenol[56]. This prototype is illustrated in Figure 15.

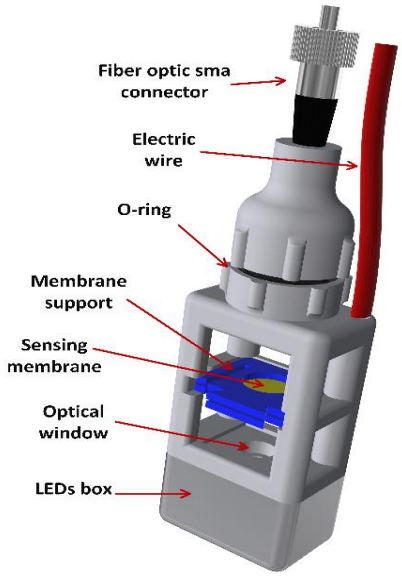

Figure 15: Sensor A that was developed for this sensor, which used fiber optics and a spectrometer[56].

For Sensor A, the method of measurement involves the optical signal being captured and collimated into a fiber optic core, which means that the signal travels along fiber optic.

The entire measured signal is impacted by impact, pressure, and other variables since a fiber optical signal is sensitive to breakage, strain, temperature change, or pressure change. This makes the use of fiber optics in an optical sensor prone to inaccuracies because it causes fluctuations in the measured values that are not caused by variations in CO_2, but rather by other external factors.

The basic detecting principle is based on two distinct optical signals being used for absorbance measurements of the sensing membrane. The light source utilized for measurements is an RGB LED that can send three independent optical signals through the sensing membrane. The blue signal is used to perform the CO_2 measurement by absorption (~470nm), while the red signal (~630 nm) is only used as a reference signal to eliminate external fluctuations. The platform was tested in different CO_2 concentrations (vs. N_2) ranging from 0% to 100%.

4.2. Development of Sensor B

An optical system was designed to assess the color variation of the sensing membrane, where white light is transmitted through a colorimetric membrane by using a white LED

(model c503d, United Kingdom) and captured by a Si photodiode (s9032, Hamamatsu, Japan).

A system was designed to optimize, in a low-cost sense, an absorption measurement of a colorimetric membrane. For this objective, an optical/electronic system was encapsulated inside several structures that were designed and 3D printed.

The CO_2 concentrations are determined by the sensor using an analysis of light's absorption, with the same principle as Sensor A. While the other color signals are utilized as reference signals, the light absorption will be represented as an increase or decrease in the blue light signal of the RGB photodetector.

The transmitted signal is detected by the wavelength selective photodiode (mentioned above), which has spectrum filters for three different wavelength bands. Three signals with distinct wavelengths are separated from the white light that is emitted: Red (590-720 nm) with a peak sensitivity at 620 nm, Green 480-600 nm) with a peak sensitivity at 540nm, and Blue (400-540nm) with a peak sensitivity at 450 nm.

Figure 16 compares the emission spectra of the white LED with the detection sensitivity of the photodiode that produces 3 electrical signals.

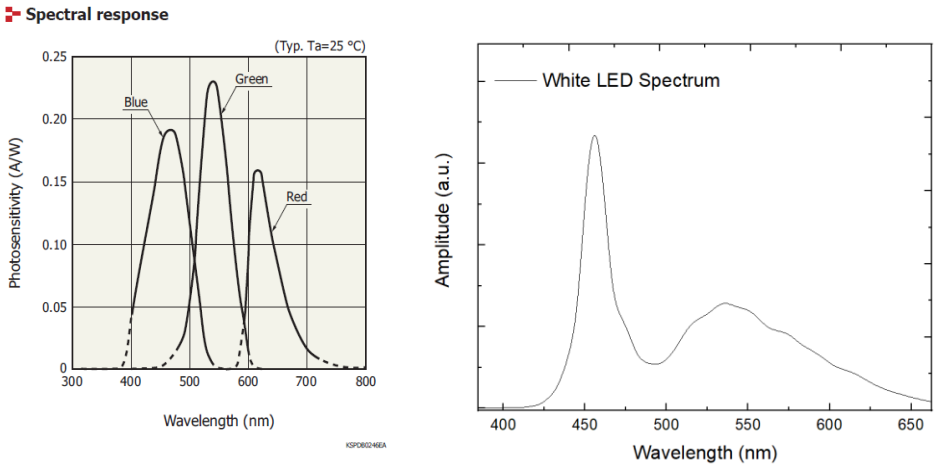

(a) (b)

Figure 16: (a)Wavelength response of the photodetector[60]. (b) White LED emission Spectrum.

The silicon-based photo diode has a small amount of exposed surface area to the white LED light. Two lenses (LC7, Roithner LaserTechnik, Austria) that collimate white LED light focus it so that it shines directly on the photodiode. Three input pins are linked to each pin of the RGB detector through a printed circuit board (PCB), which is then transformed into voltage, amplified, and read by a microcontroller.

4.3. Electrical Circuit Simulation

As a proof of concept, a simulation of this circuit was run in MultiSim (National instruments, EUA). A few current levels were evaluated together with the electrical components that would be used in the actual sensor throughout the tests. Resistance values were evaluated and modified to determine whether it would be possible to measure minute fluctuations in the input current.

The main principle is that an ideal Operational amplifier (OPAMP) has no voltage differential between the input terminals and doesn't pull current in a closed-circuit loop. Depending on the circuitry around it, an OPAMP can boost an input electrical signal. As a result, a few potentiometers might be utilized as adjustable variable resistors for each signal. Figure 17 shows a simulation of the amplification circuit that was performed.

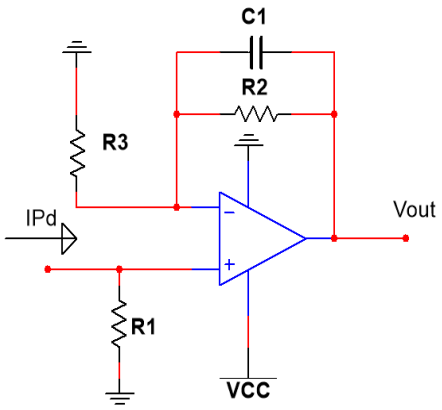

Figure 17: A schematic of the amplification circuit built around the OPAMP.

Each component is marked with a symbol to better understand the output voltage formula. The current generated by the photo diode IPd, R1 is an amplification resistor where all the current passes through to the ground. For the OPAMP, there were two input pins the V_+ and the V_- where their voltage values are kept the same. No current flows into the input terminals of an ideal Op Amp. The R2 resistor is an amplification resistor that interacts with the OPAMP, the C1 capacitor works as a frequency filter to avoid unwanted signal noise and voltage peaks. R3 resistor is a place holder for a potentiometer that works as a variable resistor to change the amplification of the signal in real time. Vout is the amplified signal that results from all the amplification and is read by the microcontroller.

The following equations can be used to derive a gain formula and an output equation[61].

$$V_+ = I_{Pd} * R1 \quad (4.1)$$

$$V_- = V_+ \quad (4.2)$$

$$V_{out} = V_+ * G \quad (4.3)$$

$$G = \frac{R2 + R3}{R3} \quad (4.4)$$

$$V_{out} = I_{Pd} * R1 * (\frac{R2 + R3}{R3}) \quad (4.5)$$

The above-calculated gain of the output voltage is dependent on the set values of each resistor in the circuit. The use of potentiometers enables for gain adjustment in case the optical signal undershoots or overshoots, saturating the readings, meaning no signal is being measured.

An integrated circuit, MAX 840 (MAXIM, Austrália), was used as a source of negative voltage (-2V) in the amplification circuit.

A variable offset of the output signal was obtained by using potentiometers in a voltage divider configuration. In the voltage divider setup, a minus two voltage source was supplied into one of the potentiometers. Due to the photodiode connection to ground and due to the on rails OPAMP, any excess voltage would not harm the overall circuit. Adding a negative tension source with a variable voltage divider gives more options when it comes to light sources and intensities.

4.3.1. Amplification Circuit

The photodiode current is amplified and converted to voltage with the primary objective of monitoring small changes in current, associated with variations in the color of the sensing membrane. Potentiometers in conjunction with OPAMP were used to build an amplification circuit that outputs an amplified and offset signal.

The key goal was to make it possible for each received signal to be calibrated with its own amplification settings. In contrast to the full light signal, the differences in color for the blue electrical signal are quite minor. To enable the monitoring of these minute variations, each signal was calibrated using a signal amplification potentiometer and another potentiometer that was coupled to a negative voltage source to be used as an adjustable offset voltage.

The fundamental benefit of having a programmable amplifier for an electrical signal is shown in Figure 18. The signal to noise ratio is low and it becomes difficult to assess or quantify the minute variances in color that are associated with changes in an electrical signal when the baseline of the overall signal is set too high.

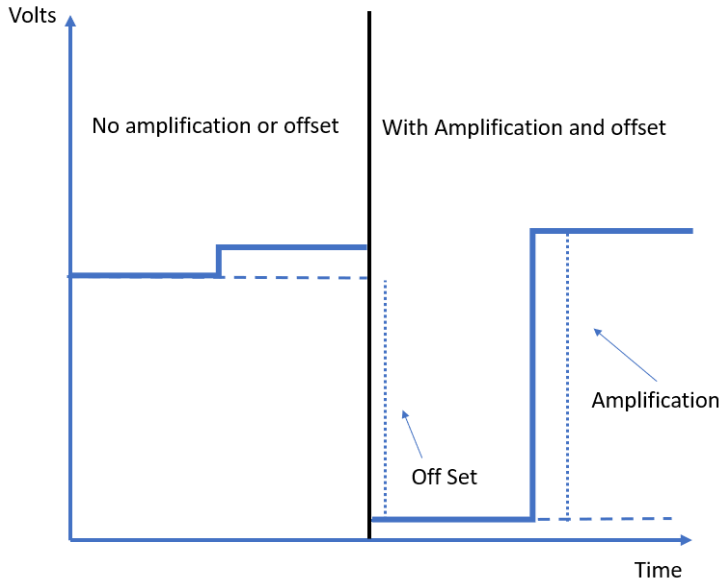

Figure 18: Graphic showing two changes in voltage levels, one without the advantage of signal amplification, and one without.

A few capacitors were used as a low pass filter to avoid unwanted peaks and noise from electrical signals. The microcontroller linked to the printed circuit board is shown in figure 19 (a). At the surface, there are 6 potentiometers that are used to adjust the output signal. Figure 19 (b) is the underside of the printed circuit board, where the amplification of the photo diode current occurs.

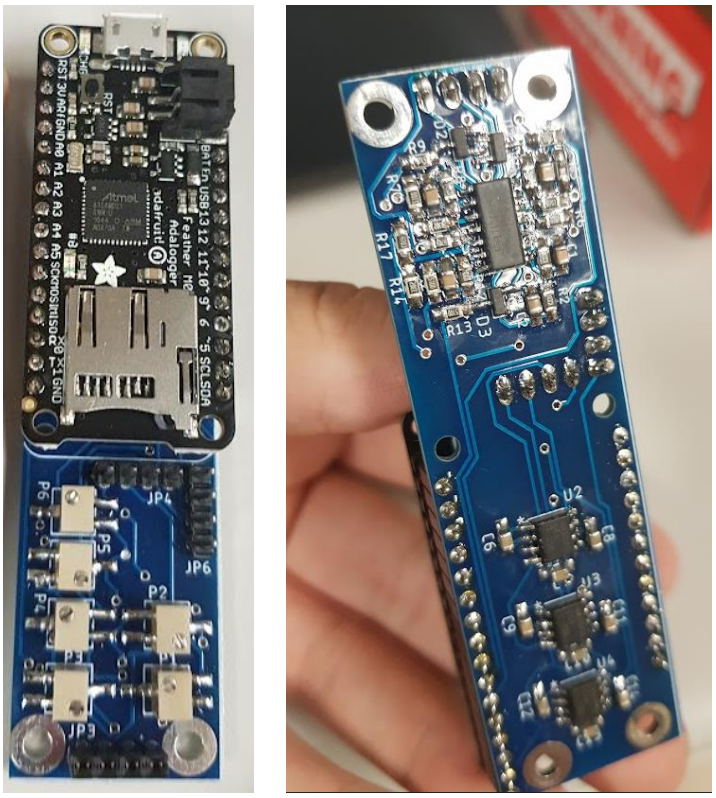

(a) (b)

Figure 19: (a)Printed circuit board of the amplification circuit with an Arduino feather m0 inserted a side. (b) Back side of the PCB.

Because the generated currents were so small, it was necessary to use the smallest electrical connections possible, to avoid the possibility of electrical noise affecting the captured signal.

4.3.2. Quantification

The output of an optical signal was transformed to an electrical signal with a voltage range of 0 to 3.3 volts. To read this electrical signal and transform it into a quantifiable signal, a microcontroller with an analog to digital converter (ADC) was used. Quantifying the signal was done with a 10-bit ADC. The amplification circuit's continuous voltage was turned into a discrete reading, which the microcontroller displays as a series of integer values. With each increase in the number of accessible bits, the Max value reading increases and resolution improves.

$$Max\ Value = 2^{number\ of\ bits} - 1 \qquad 4.6$$

The Max Value is doubled for each additional bit. The resolution is related to the number of bits available, therefore as the number of bits grows, the resolution improves.

$$Resolution = \frac{V_{max} - V_{min}}{2^{nbits}} \quad 4.7$$

V_{max} is the highest voltage value, which in this case is 3.3 volt, while V_{min} is the lowest value, 0 volts. V_{max} and V_{min} are forced by the on rails OPAMP.

Oversampling was used to program the microcontroller to enhance the number of effective accessible bits for the ADC. An increase in one bit, means that each measurement is read at least 4 times. An increase in two bits, means that each measurement is read at least 4^2 times.

$$F_{OverSampling} = (4^{nbits}) * F_s \quad 4.8$$

Because the value measured by the ADC does not have a unit, each graphic refers to this output value as "Amplitude," using arbitrary units (a.u.). The sensor's measurements are given as a sum, not as a spectrum, the value given as no inherent meaning.

4.3.3. Temperature Monitoring

Temperature is a significant variable that can affect the CO_2 detection system response. The response of the entire system might change depending on temperature fluctuations; hence temperature monitoring is crucial.

A 10k negative temperature coefficient (ntc) thermistor was attached to a micro controller to monitor temperature.

A circuit with a 10 kΩ reference resistor was designed to use this thermistor. A voltage divider circuit was mounted in the sensor using a micro controller has a voltage source, voltage meter and ground. Figure 20 shows the circuit built to measure temperature using the thermistor.

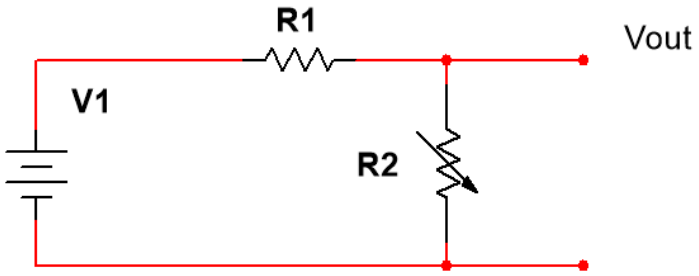

Figure 20: Thermistor electrical Circuit.

For the Tension source, the microcontroller 3.3 volt pin out was used ($V1$), the reference 10kΩ resistor is $R1$, $R2$ is the thermistor itself. V_{out} was connected to an analog read pin of the microcontroller and the other pin connected to ground.

The voltage readings of the thermistors are translated into resistance and subsequently into temperature using the following formulae.

$$V_{out} = V_1 * (\frac{R_2}{R_1 + R_2}) \quad 4.9$$

$$R_2 = R_1 * (\frac{V_{out}}{V_1 - V_{out}}) \quad 4.10$$

Because the sensor uses an ntc thermistor, its internal resistance decreases as the temperature rises.

The voltage is transformed to resistance, which is then transferred to temperature using the Steinhart and Hard equation[61].

$$T(R) = (A_1 + B_1 \, ln \, ln \, \frac{R}{R_{ref}} + C_1 \, ln \, ln \, \frac{R}{R_{ref}}^2 + D_1 \, ln \, ln \, \frac{R}{R_{ref}}^3)^{-1} \quad 4.11$$

The thermistor datasheet contains the elements of the equation (A1, B1, C1, D1), which return the temperature in kelvin.

To calibrate the thermistor, a temperature linear fit was performed using an incubator with a temperature controller. A comparison was made between the measured and the actual temperature. Temperatures ranging from 28 to 45 degrees Celsius were chosen. These temperatures were used to determine the sensor's measuring range; higher temperatures could damage the microcontroller or chemical membrane; lower temperatures were not recorded owing to incubator limits. Figure 21 shows the comparison between measured temperature and the real value.

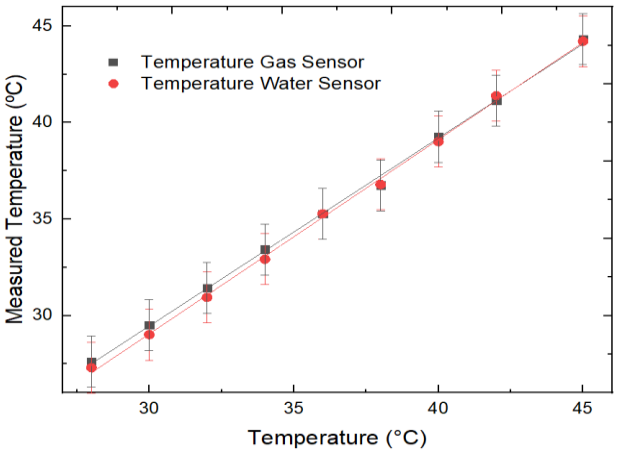

Figure 21: Temperature measured by the thermistor in both sensors vs the temperature marked by the incubator.

In order to compare the temperature values received by the thermistor circuit and an actual value generated by an incubator, data was collected and adjusted linearly as shown in Figure 21. The linear fit was achieved by isolating the sensor and avoiding external noise. The incubator was kept at the same temperature for 5 minutes after each measurement to ensure that the temperature inside was uniform. For two sensors, one for gas and the other for dissolved CO_2, two calibrations were done.

Table 2: Linear fit values of slope and intercept, along with the r square factor with the according standard deviation.

Y=mx + b	m	Δm	b	Δb	R^2
Temp Gas	0.974	0.0138	0.238	0.506	0.998
Temp Water	1.006	0.0134	-1.14	0.492	0.998

The thermistor's deviations can be traced to the reference resistor not being exactly 10k ohms; The error bars were calculated using the following formula that comes from the datasheet:

$$\Delta T = \frac{Z}{TCR} \tag{4.12}$$

$$Z = \left(\left[1 + \frac{X}{100}\right] * \left[1 + \frac{Y}{100}\right] - 1\right) * 100\% \tag{4.13}$$

Where X is the value of the reference resistor, in this case 10kohm, Y is the resistance deviation due to b tolerance and TCR is a labeled coefficient temperature.

4.3.4.Sensor B Enclosure

An enclosure was created to shield the electrical components of the sensor from environmental damage and to prevent external variables from interfering with results. Support parts were developed in Autodesk Inventor 2022 and 3D printed to design the sensor box (Zortax M2000;material:Z-Ultra T, based on ABS; Poland). Each piece was created to keep the optical system in a stable and robust configuration, with the primary goal of creating a waterproof sensor.

Figure 22 displays a diagram of every element of the sensor, including the optical system, the printed circuit board, and the microcontroller.

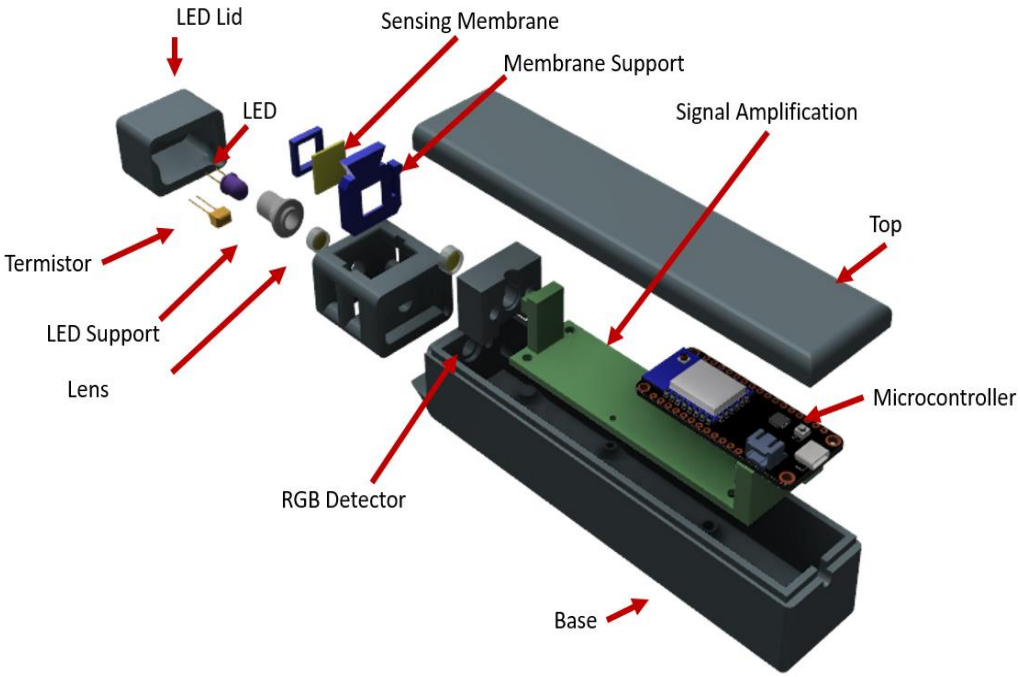

Figure 22: Autodesk Inventor 3D model render of each component of the Sensor B.

The sensor enclosure was made from a few 3D printed parts, each with the goal of supporting and constructing an optical system. After print, each piece was fixed by using epoxy. While all electronic components, including the acquisition, the signal capture/ amplification are separated.

The optical system constituted by the white LED and 2 collimating lenses, a RGB detector and a colorimetric membrane that needed to be properly aligned, in a transmission configuration. The light from the LED must be aligned with two lenses, pass through the detecting membrane, and reach the light detector. Inside the LED lid box the white LED and

one thermistor for temperature monitoring were insulated with an epoxy and glued to the sensing membrane support.

A support piece was employed to ensure and guarantee alignment and an appropriate focal distance between the first lens and the LED support. The white LED is aligned with the lens and at the focal distance of the respective lens thanks to an LED support piece.

Despite the use of epoxy to seal every slit of the 3d printed pieces, the 3D printer material itself is porous meaning it can leak water.

To waterproof each piece of the sensor box, acetone was used on each exterior surface to melt the 3D printed material fibers (ABS) into each other, sealing off the interior[62].

To further waterproof each item and ensure a tight seal, a layer of hydrophobic paint was applied.

4.3.5.Communication between systems

In Sensor B, real-time communication takes place between the computer and the microcontroller via serial communication ports. To interface with the microcontroller, a LabVIEW program was used that sends in real time commands that are preprogrammed in the microcontroller.

The micro controller functions as a power source, and the 3.3 V pin powers the rest of the PCB. The amplified signal is connected to an analog read pin.

While inactive, the Arduino code waits for a command from the LabVIEW program, that turns on the LED and provides a reading. This command is preprogrammed into the Arduino code which includes turning on the LED, reading the signals, writing the signals, and shutting off the LED. The sampling period is specified by the LabVIEW code, during which a set number of samples are collected by the Arduino code and an average is computed. Each reading returns a number between 0 and 4095.

Two sensors were developed, one of which converts an optical signal into an electrical current that is subsequently processed and amplified. A spectrometer is used by the other to analyze an optical signal. The following chapter examined the capability of each of these sensors to identify and quantify CO_2.

Chapter 5 Experimental Results

5. Sensor A and Sensor B

In this chapter we compare the performance of the Sensor A and Sensor B. Both the Sensor A and the Sensor B were tested for gaseous CO_2 and Sensor B was tested in dissolved CO_2. The data displays some of the problems that needed to be fixed during the measurements. Reversibility is shown by repeating the identical data points in both an increasing and a falling concentration for the Sensor B. For gaseous carbon dioxide, both Sensor A and Sensor B underwent calibration.

5.1. Measurements in Real-time

Two optical signals are captured, processed, and analyzed to create a correlation between optical variations and CO_2 concentrations. To process the changes along wavelength and amplitude of both signals, an integral is calculated in real-time. This method was used by both Sensor A and Sensor B. The representation of these values in real-time was called the timeline, where the red wavelength and the blue wavelength are integrated to offer two values which change over time.

An example of how the data is presented is shown in figure 23.

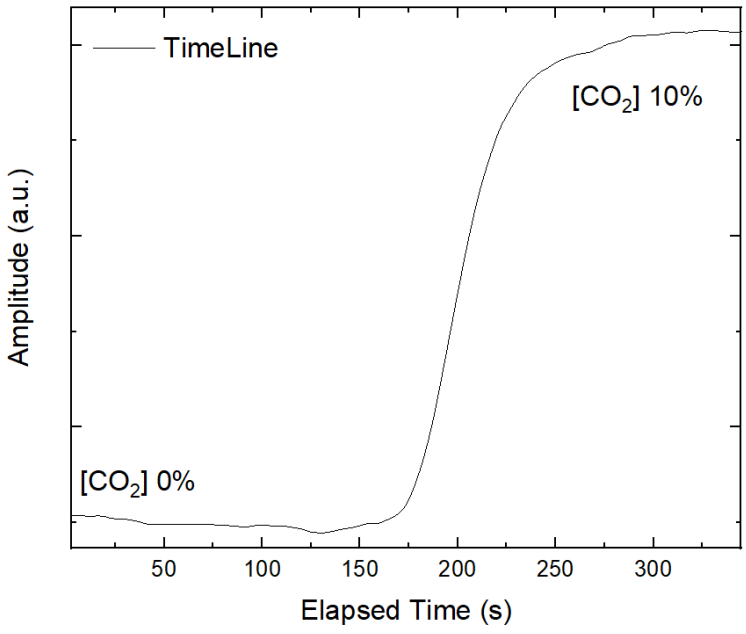

Figure 23: Real-time visualization of the sensing optical response

A lower concentration of "0%," which represents a 100% of nitrogen atmosphere, and a higher concentration of 10% CO_2 in N_2, were both applied to the Sensor A and the Sensor B in Figure 23. The graph displays the change in the blue signal concentrations over time as they occur in real-time.

The increase in signal strength reflects the physical change of the yellow membrane losing color due to an internal chemical reaction, and all next data will be presented in a similar form. For more accurate measurements a corrected signal is presented where:

$$Sensing\ Signal = 1000 * \frac{Integral\ of\ Blue\ Signal}{Integral\ of\ Red\ Signal} \quad 5.1$$

The sensing signal has no units due to it being a quotient of two optical signals. The multiplication by the value of 1000 facilitates comparison with the values that the ADC outputs, which are between 0 and 4000. Since these values have no units behind them, some graphs will not present the values themselves to avoid confusion.

5.2. Sensor A Data

The primary goal of Sensor A is to reduce the size of the Sensor A and streamline its operation by eliminating the need for a spectrometer, so data from the Sensor A is shown to contrast with the Sensor B. Data obtained with Sensor A, uses a more sensitive transducer that is described in[56].

5.2.1. Gas flow effect

A study was carried out on the sensor response to different gas flows.

During measurements a constant flow of gas was kept assuring a steady substitution of the gas inside the measurement chamber. In this case concentrations of 0% and 100% of CO_2 were considered to ensure the maximum variations on the optical response. Two different set of cycles between those concentrations using flow rates of 500 and 1000 ml/min were compared. Figure 24 shows the optical response to the different flow rates.

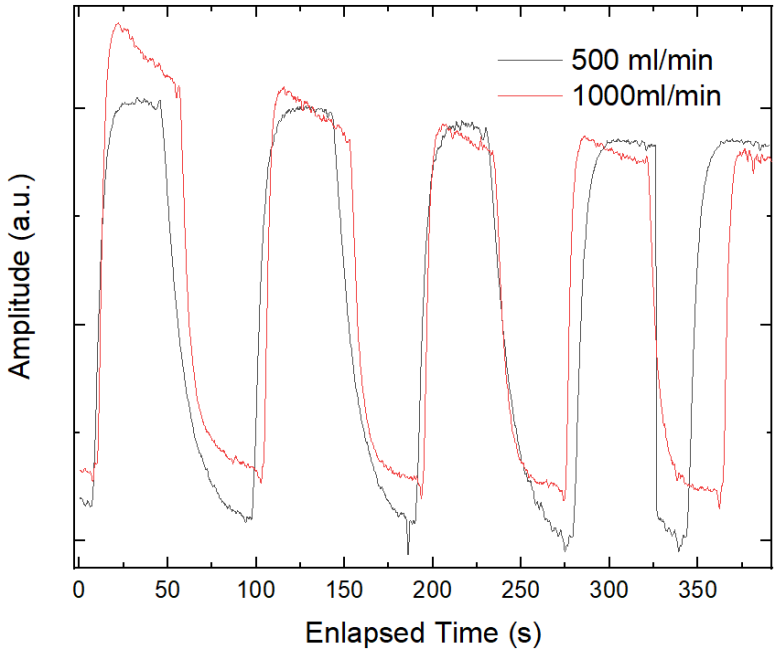

Figure 24: In a measurement chamber, two gas flows were examined using alternating atmosphere cycles.

The greater gas flow of 1000 ml/min results in a steady decrease in the sensing signal, whereas the lower flow maintains a more stable signal overall.

A probable cause for this effect is that the flow is too high to allow the internal chemical reactions to stabilize. Another cause might be the membrane being the flow drying the chemical reagents that compose the membrane.

This explains why a constant flow of 500 ml/min was used for all additional measurements in the next chapter.

5.2.2. Calibration in Gas

A calibration was performed with Sensor A where a range between 1% and 3% CO_2 was used. Figure 25 shows the spectrum of each concentration measured.

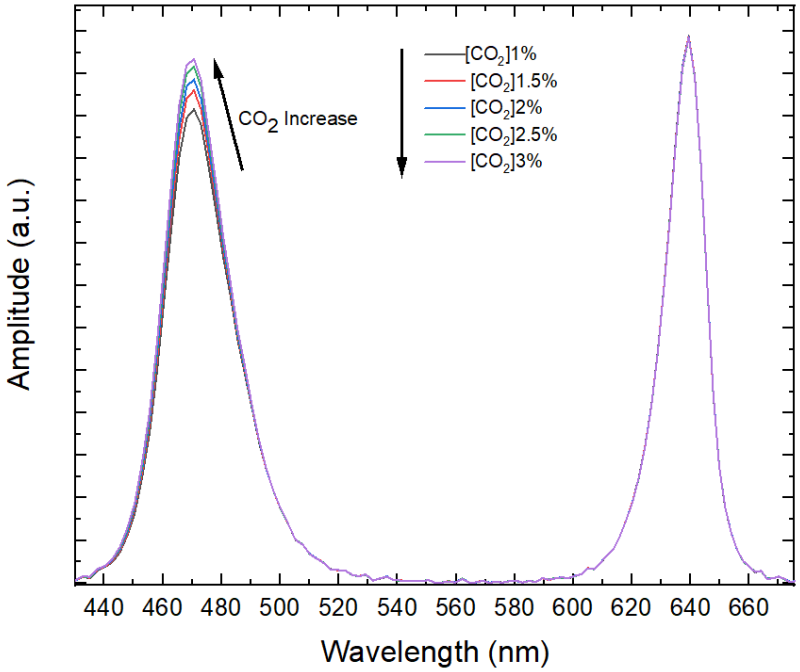

Figure 25: Spectrum of the different levels of CO_2 that were measured, in the calibration.

As the exposure to higher levels of CO_2, the amplitude of the sensing signal (470nm) increased, while at the same time the reference signal (630nm) had no significant changes. Figure 26 shows the measurement timeline as well as the repeated measurements of each concentration level.

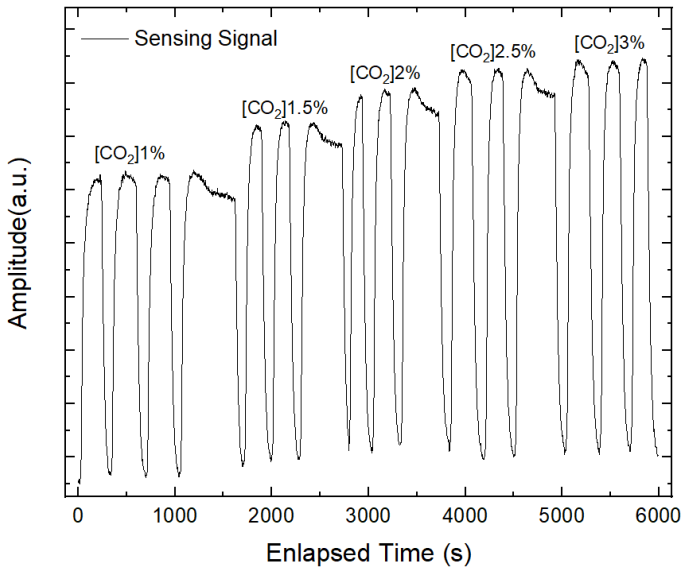

Figure 26: Timeline of a calibration, where each concentration was repeated at least 3 times.

In this calibration, the measuring chamber was mostly emptied of CO_2 by using purges N_2 so that air inside the measuring chamber was quickly substituted.

After each level was taken, the whole response from near 0% CO_2 to the concentration was monitored.

This method was used to check whether the sensor was consistently measuring the same readings for the same concentrations. Each concentration was repeated three times.

Sensor A was calibrated using a linearization as seen in figure 27, where a logarithmic scale with a base e was employed.

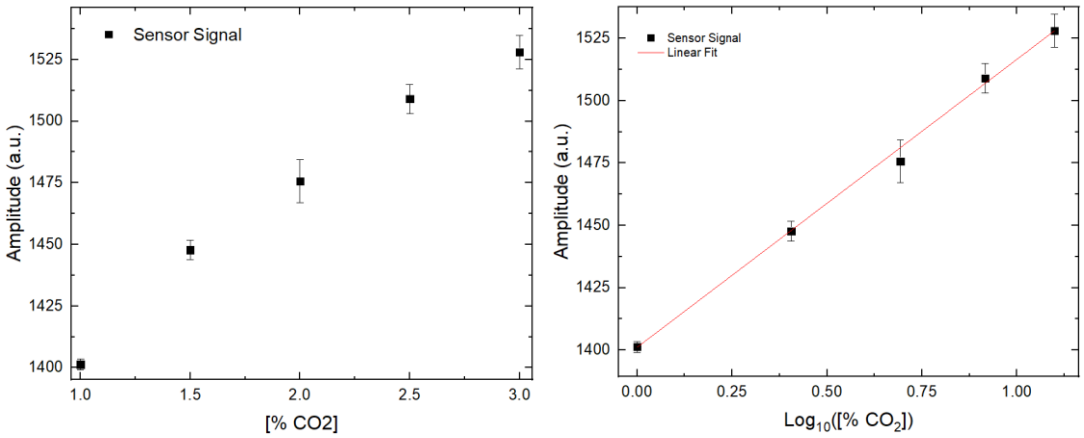

(a) (b)

Figure 27: (a) Average of concentration levels. (b) Linearization of data.

The linearization parameters were used to determine the limits of detection (LOD) and limit of quantification (LOQ) displayed in table 3 using the following equations:

$$LOD = b_0 + 2 * t_{95}^{u} * \sigma_b \quad 5.2$$

$$LOQ = b_0 + 3 * 2 * t_{95}^{u} * \sigma_b \quad 5.3$$

Where b_0 is the intercept parameter, σ_b is the standard deviation and $t_{95}^{u}$is a critical value following the t-Student distribution.

Table 3: Calibration of Sensor A linear fir parameters.

	Intercept(b)	**Slope (a)**	**R-Square**	**LOD (CO_2%)**	**LOQ (%CO_2)**
y= a + b*x	1401.2± 0.9	115±2	0.9991	1.07	1.23

The limit of detection of Sensor A, which means the lowest amount it can detect is high when considered a measuring range between 1 to 3 % CO_2.

Modified environment packaging may be viable application for this sensor in this measurement range. Based on previous research this sensor was tested for aquaculture[56].

5.3. Sensor B Results

A Sensor B was developed that removed the requirement for fiber optics and a spectrometer, making it easier to operate.

5.3.1. Reversibility study

Reversibility is the capacity of a sensor to repeatedly inject it with the same gas concentrations and measure the same signal. Cycles with alternate injections of two distinct concentrations were carried out to analyze the stability of the measurements over time and evaluate if the detecting signal was able to self-recover. Figure 28 shows the stability of the signal.

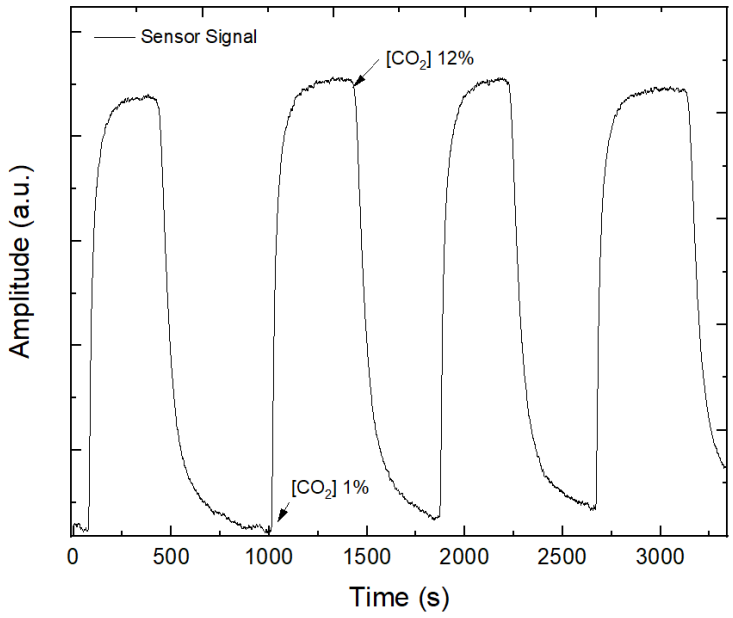

Figure 28: Response of the sensor with different cycles of concentrations between 1% CO_2 and 12% of CO_2.

Different cycles were performed, where the sensor was exposed to two gaseous concentrations of CO_2,1% and 12% respectively. These injections were performed with

constant influx of 500 ml/min, where for 1% (5ml/min of CO_2 and 495 ml/min of N_2) and 12% (60ml/min of CO_2 and 440 ml/min of N_2).

Repeated measurements were performed of the same two concentrations of CO_2, the sensor was able to recover its signal multiple times, which means the chemical membrane was able to recover its color. This proves the chemical process is reversible.

5.3.2. Hysteresis Analysis

A reversible sensor can measure the concentrations of carbon dioxide when it is going from a lower to a higher concentration of carbon dioxide, or otherwise measuring from a high concentration to a lower concentration. A test was performed to compare the performance during the rise and during the fall of CO_2 concentration. The sensor was exposed to concentrations from 1% to 12% of CO_2 during at least 5 minutes to give the signal time to stabilize. The results with the increasing and decreasing of CO_2 concentration are in figure 29.

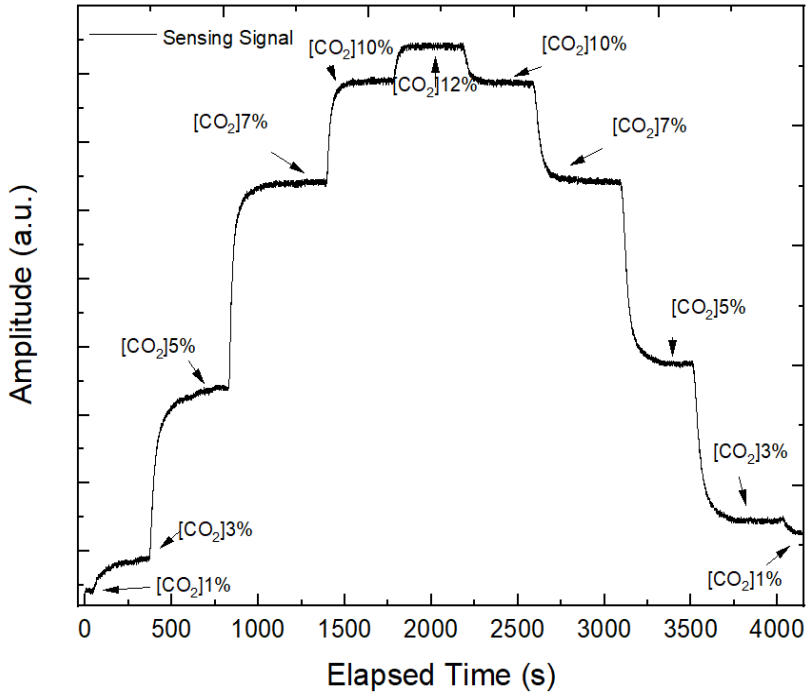

Figure 29: Response of Sensor B to varying CO_2 concentrations in increments of 2%, ranging from 1% to 12%.

Once the 12% concentration produced a steady signal, lower concentrations were injected in real-time, decreasing from the highest concentration to the lowest. An injection was done for at least 7 minutes as each concentration decreased.

To properly conduct the experiment, the increase and fall of the concentrations were injected three times in a row. For each stable level of CO_2 concentration observed, an average was determined. For each level, 400 points were averaged, and this equals one point in figure 30.

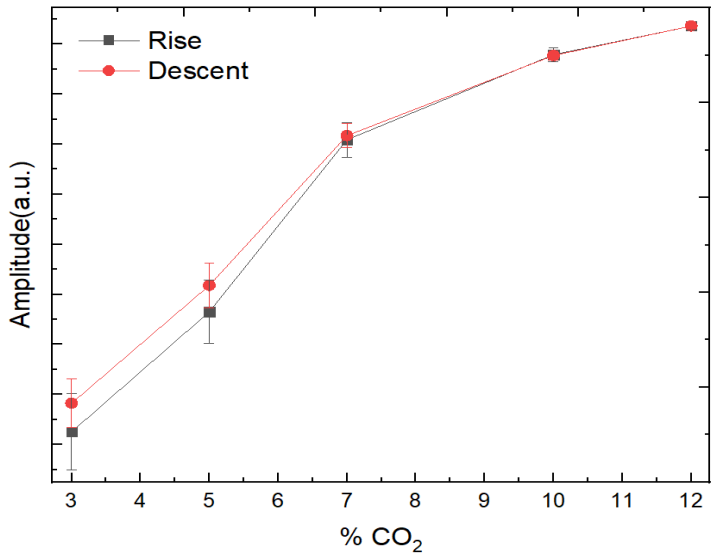

Figure 30: The average of each concentration level measured and compared.

For this hysteresis cycle, a small drift for lower concentrations was observed. Which means the sensor is more stable for higher concentrations.

5.3.3. Calibration Curve of the Sensor B

A calibration curve is needed for the built-in sensor to connect changes in an optical signal into a measurement of carbon dioxide levels. For a sensor to make measurements it needs a calibration curve, which converts the detected signal into a readout of gas concentrations. This calibration curve has to be properly developed and examined in order to verify a sensor's properties. The measurement range was set between 7% and 20%. This range was selected because, as seen in the previous chapter, the sensor is more stable at higher concentrations while exhibiting a hysteresis effect at lower concentrations.

Each gas concentration was injected for at least 5 minutes to allow for a stable signal. Each concentration was higher than the previous one, creating a cumulative signal.

Figure 31 illustrates each concentration that was injected into the measurement chamber as well as the consistency of each level.

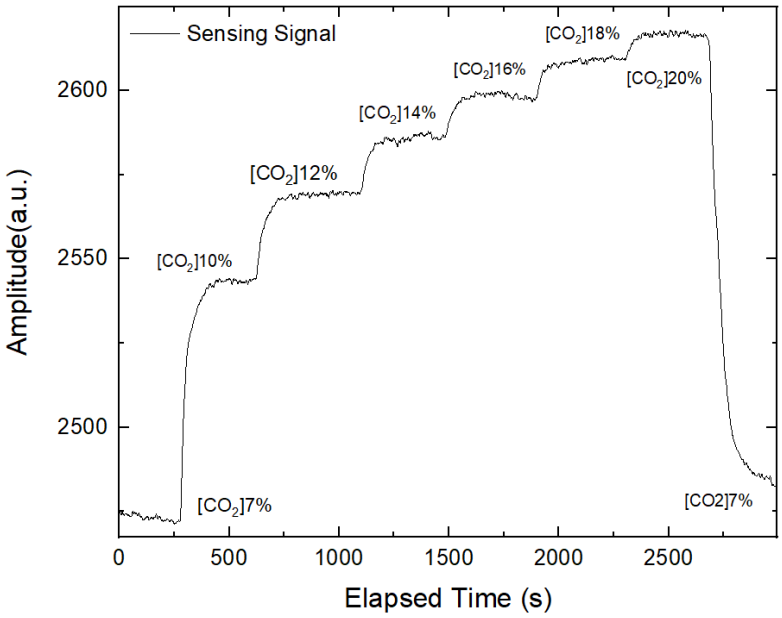

Figure 31: A cumulative cycle that was performed to calibrate the sensor, where an ever-increasing level of concentration was injected.

These cumulative cycles were performed multiple times, to ensure that the levels measured were stable, just as shown in figure 32.

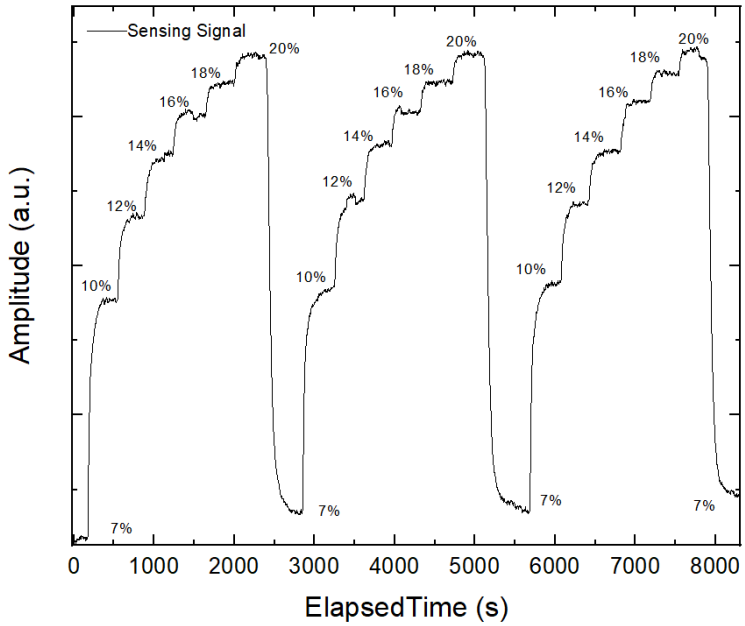

Figure 32: Real-time measurements of 3 cycles of a calibration.

After reaching a concentration of 20%, an injection of 7% was performed between the following measurements so the signal recovers a level that was used as a baseline. The injection of the lower concentration of 7% was performed for 15 minutes.

This process was repeated 3 times for each concentration. This to make sure that all measurements are viable and repeatable. The average of all 3 repetitions was calculated.

A linearization of the calibration data was performed in figure 33, by using the logarithmic scale of base 10.

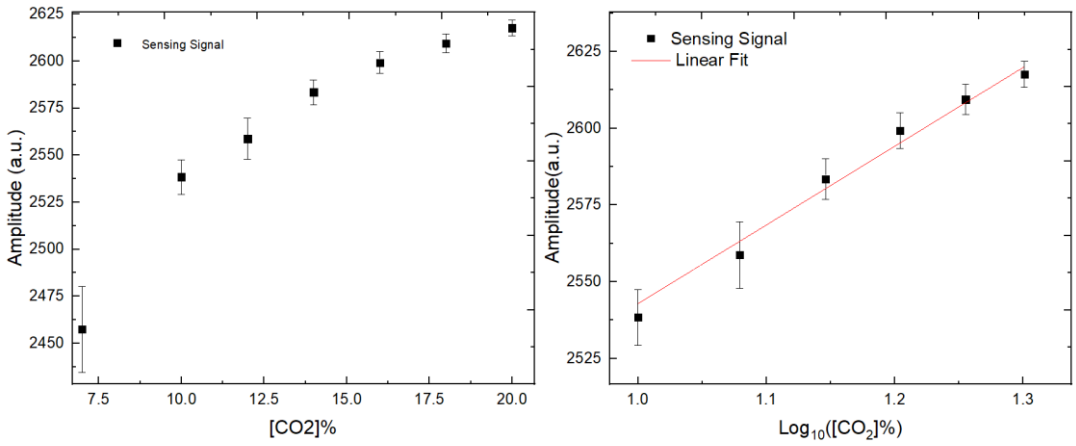

Figure 33: (a) The average calculated of optical signal for each concentration level. (b) Linearization of the calibration data.

This is crucial for determining the sensor's detection and quantification limits, with this linearization the LOD, and LOQ was calculated in table 4.

Table 4: Calibration of Sensor B linear fit parameters.

	Intercept(b)	**Slope (a)**	**R-Square**	**LOD (CO_2%)**	**LOQ (%CO_2)**
y= a + b*x	$(2.28 \pm 0.02) \times 10^3$	$(2.6 \pm 0.2) \times 10^2$	0.982	1.87	6.61

Gaseous CO2 measurements from Sensor B ranged from 7 to 20%. The limit of detection of Sensor B is 1.87%, which is the smallest detection that by definition can be achieved. Modified environment packing or storage may be a good application for this measuring range.

5.4. Dissolved CO_2 Measurement

The same methodology was applied in the measurement of CO_2 dissolved in deionized water through a twin sensor with optoelectronic properties optimized for under water application.

Since the aquatic environment acts as a magnifying glass and increases the sensitivity of the optical signal when compared to a gaseous environment, sensor B needs to be calibrated specifically for water measurements.

A higher sensitivity brings some disadvantages, when the signal is too sensitive, any form of obstruction, whether be dirt/dust/Air bubbles, can either saturate the signal or eliminate it. The optical signal easily saturates or produces low values, which makes calibration more difficult.

Due to signal saturation, a sensor calibrated for a gaseous environment cannot function in an aqueous environment. Another drawback is the possibility that the Sylgard 184 might tear or fail to encapsulate the chemical membrane, which would cause the signal to get saturated and inhibit the membrane from forming stable chemical reactions with CO_2.

5.4.1.Dissolved CO_2 Calibration

A commercial Portable CO_2 Analyzer (Oxygard, Farum Denmark) was used to calculate the calibration given in figure 34 to determine how much CO_2 was dissolved within the water filled measurement chamber.

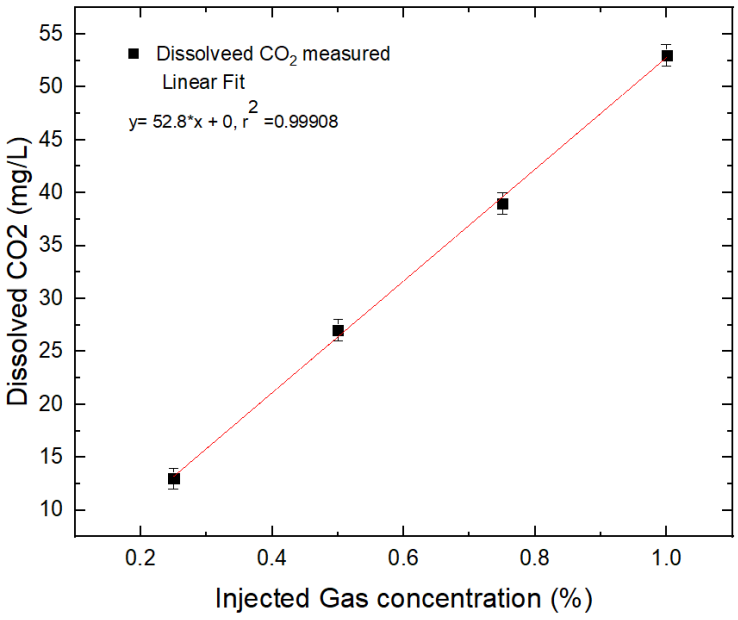

Figure 34: Linear fit correlating gas injections(concentrations in percentage) with dissolved CO_2 concentrations

A linear dependence was observed between the gas concentrations that were being injected and the amount of dissolved CO_2 inside the water filled measurement chamber.

The linear fit was used to measure the lowest concentration of dissolved CO_2 that sensor B was able to detect. The dissolved CO_2 readings for injections of greater CO_2 concentrations were unknown due to the Oxyguard sensor's limitations.

5.4.2. External Perturbations and Reversibility

One of the main challenges of measuring underwater with an optical signal is the presence of air bubbles/dust that are formed by injecting gas into the water. The abrupt change in refractive index changes the optical path direction and creates abrupt changes in the real-time measurement signal. In figure 35, it shows cycles of alternating concentrations were performed in an aqueous environment.

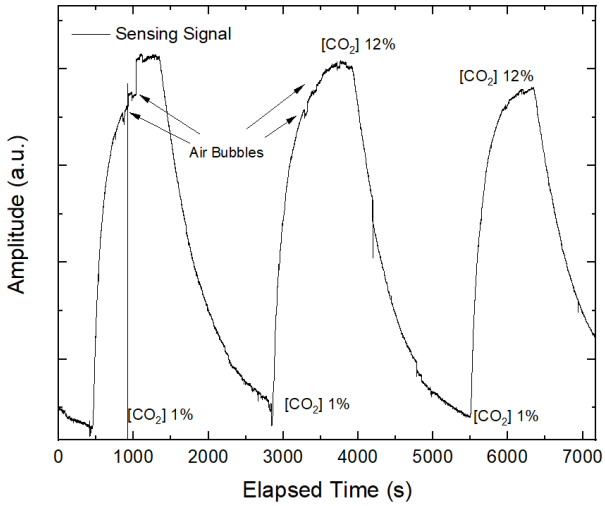

Figure 35: Cycles of alternating dissolved CO_2 concentrations.

For 15 minutes, gas injections were done to change the dCO_2 concentrations. The lowest level measured by Sensor B was 50 ppm, according to the collected data by the dissolved CO_2 sensor Oxygard.

Since the sensor is colorimetric, a membrane is used and air bubbles tend to be trapped under the sensor, figure 35 shows the effects of smaller bubbles that changes the real-time signal that is measured. Since small bubbles accumulate, depending on the size of the bubbles the signal will either drop slightly or drop completely. The sensor is taken out of the measuring chamber, tilted, and then put back in to remove the air bubbles.

Cycles were performed of alternating concentrations of dissolved CO_2 to test if the sensor can recover its signal with multiple injections. This is a way to test the reliability of its performance.

Tests were performed to evaluate the capacity for the sensor to recover its signal with repeated measurements in real-time of concentration, this is shown in figure 36 multiple times.

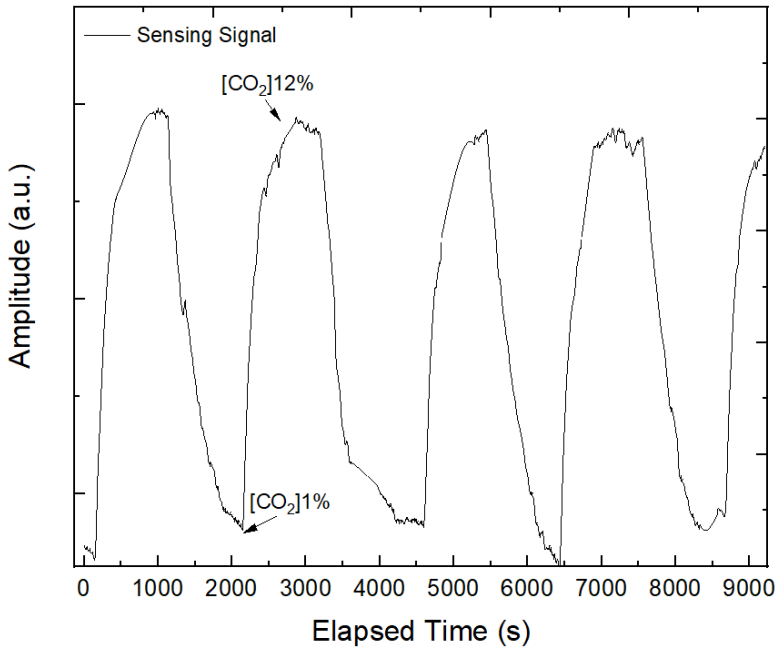

Figure 36: Timeline of alternating cycles between injections of 1% CO_2 and 12 %CO_2.

During measurements some air bubbles were caught by the sensor and had to be edited out of the data. Since the sensing signal is ratiometric, when air bubbles are caught the values tend to go to infinitum. After each measurement, the chemical membrane was able to regain its color, which matched the results for gaseous CO_2 behavior. These results show that dissolved CO_2 reactions take substantially longer than gaseous CO_2 reactions to complete.

5.4.3.Differentiating Concentrations levels of dCO_2

One important factor for a sensor is the ability to differentiate between different concentrations. Preliminary data was obtained to see the capabilities for this with 6 different concentration levels. Figure 37 shows the Sensor A ability to distinguish between concentrations of dissolved CO_2. Due to specific restrictions, only the lowest concentration of dissolved CO_2 is known; the other four values are unknown.

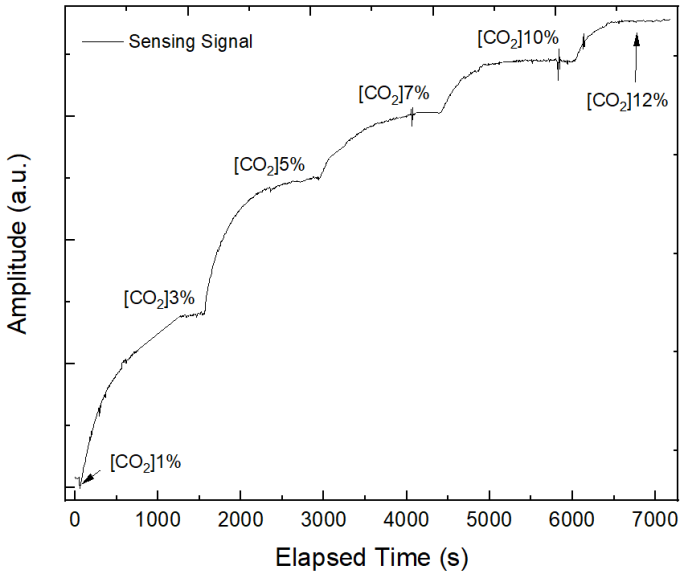

Figure 37: A cumulative cycle that was performed to calibrate the sensor for dissolved CO_2, where an ever-increasing level of concentration was injected.

With a measurement range between injections of 1% CO_2 and 12 % CO_2, the Sensor A was able to discriminate between different dissolved CO_2 concentrations. The signal tends to saturate at higher doses.

Chapter 6 Conclusions and Future Work

The major goal of this project was to develop an optical sensor that was compact and could be utilized with little setup from the user, where color fluctuations were the primary means of measuring.

Both dissolved CO_2 in water and gaseous CO_2 in the atmosphere were evaluated using Sensor A, which was developed in earlier studies. To create a more affordable, compact, and miniaturized version, Sensor B was fully developed in this thesis. Both sensors use the absorption measurements for their sensing methodology; the way in which they capture light differs, and the signal processing is different, also the sensing layers are based on different chemistry.

Both sensors coarsely evaluated in the full concentration range. And following preliminary tests, the sensors were tested in more detail in the ranges were their performances was best.

For gas measurements, the Sensor A was characterized in a range between 1% and 3% CO_2, with a limit of detection of 1.07% and a limit of quantification of 1.23 % CO_2. However this limited range is because the sensor was optimized for aquaculture where the dissolved concentrations are at the parts per million level.

For Sensor B, a characterization was performed for ranges between 7% and 20% CO_2, with a limit of detection of 1.87% and a limit of quantification of 6.61% CO_2. For sensor B for this measurement range might be used for atmosphere food packing and storage.

Sensor B was also tested for dissolved CO_2 concentrations, but due to limitation of equipment the dissolved concentrations were unknown. Nevertheless, for dissolved CO_2 concentration, Sensor B should use the same colorimetric transducer as sensor A.

Both sensors showed promise for application in some industries, sensor B was based on sensor A, miniaturized while retaining the similar functions. Sensor A used a more sensitive version of the colorimetric transducer, in principal if the same transducer is used in sensor B, similar results could be obtained in a more compact configuration.

This demonstrates the sensor's modularity as it maintained same operating mechanism while being heavily modified and simplified.

According to early results, sensor B may be employed for dissolved CO_2 applications. Sensor A was previously used for these purposes in previous research. A better gas system is still required to assess reaction times. Due to its modular structure, Sensor B's amplification circuit and design may be further enhanced, further shrunk, wireless

communication, and more compressed in further development. With further work, its application field may be expanded.

References

[1] M. Ades *et al.*, “Global Climate,” *Bull. Am. Meteorol. Soc.*, vol. 101, no. 8, pp. S9--S128, 2020, doi: 10.1175/BAMS-D-20-0104.1.

[2] D. Nong, P. Simshauser, and D. B. Nguyen, “Greenhouse gas emissions vs CO2 emissions: Comparative analysis of a global carbon tax,” *Appl. Energy*, vol. 298, p. 117223, 2021, doi: 10.1016/j.apenergy.2021.117223.

[3] D. J. Hofmann, J. H. Butler, and P. P. Tans, “A new look at atmospheric carbon dioxide,” *Atmos. Environ.*, vol. 43, no. 12, pp. 2084–2086, 2009, doi: 10.1016/j.atmosenv.2008.12.028.

[4] P. M. Vitousek, H. A. Mooney, J. Lubchenco, and J. M. Melillo, “Human Domination of Earth’s Ecosystems,” in *Urban Ecology*, Boston, MA: Springer US, 2008, pp. 3–13. doi: 10.1007/978-0-387-73412-5_1.

[5] “Gas sensor market size to reach $1.3 bn by 2027 at CAGR 6.4%,” *Focus Catal.*, vol. 2021, no. 5, p. 2, 2021, doi: 10.1016/j.focat.2021.04.009.

[6] A. D. Dukes III, “Measuring the Henry’s Law Constant for Carbon Dioxide and Water with UV-visible Absorption Spectroscopy,” *Anal. Sci.*, vol. 36, no. 8, pp. 971–975, Aug. 2020, doi: 10.2116/analsci.19P477.

[7] K. Gao, J. Beardall, D.-P. Häder, J. M. Hall-Spencer, G. Gao, and D. A. Hutchins, “Effects of Ocean Acidification on Marine Photosynthetic Organisms Under the Concurrent Influences of Warming, UV Radiation, and Deoxygenation,” *Front. Mar. Sci.*, vol. 6, 2019, doi: 10.3389/fmars.2019.00322.

[8] L. Cao, K. Caldeira, and A. K. Jain, “Effects of carbon dioxide and climate change on ocean acidification and carbonate mineral saturation: Climate change on Ocean Acidification,” *Geophys. Res. Lett.*, vol. 34, no. 5, 2007, doi: 10.1029/2006GL028605.

[9] B. A. Seibel and P. J. Walsh, “Biological impacts of deep-sea carbon dioxide injection inferred from indices of physiological performance,” *J. Exp. Biol.*, vol. 206, no. 4, pp. 641–650, 2003, doi: 10.1242/jeb.00141.

[10] J. C. Orr *et al.*, “Anthropogenic ocean acidification over the twenty-first century and its impact on calcifying organisms,” *Nature*, vol. 437, no. 7059, pp. 681–686, Sep. 2005, doi: 10.1038/nature04095.

[11] R. A. Feely *et al.*, “Impact of Anthropogenic CO 2 on the CaCO 3 System in the Oceans,” *Science (80-.).*, vol. 305, no. 5682, pp. 362–366, Jul. 2004, doi: 10.1126/science.1097329.

[12] B. G. Smith, “Developing sustainable food supply chains,” *Philos. Trans. R. Soc. B Biol. Sci.*, vol. 363, no. 1492, pp. 849–861, 2008, doi: 10.1098/rstb.2007.2187.

[13] B. Gilland, “World population and food supply,” *Food Policy*, vol. 27, no. 1, pp. 47–63, 2002, doi: 10.1016/S0306-9192(02)00002-7.

[14] G. S. Lorite *et al.*, “Novel, smart and RFID assisted critical temperature indicator for supply chain monitoring,” *J. Food Eng.*, vol. 193, pp. 20–28, 2017, doi: 10.1016/j.jfoodeng.2016.06.016.

[15] I. J. Church and A. L. Parsons, “Modified atmosphere packaging technology: A review,” *J. Sci. Food Agric.*, vol. 67, no. 2, pp. 143–152, 1995, doi: 10.1002/jsfa.2740670202.

[16] B. A. Blakistone, Ed., *Principles and Applications of Modified Atmosphere Packaging of Foods*. Boston, MA: Springer US, 1997. doi: 10.1007/978-1-4615-6097-5.

[17] W. E. Muir, D. Waterer, and R. N. Sinha, “Carbon Dioxid as an Early Indicator of Stored Cereal and Oilseed Spoilage,” *Trans. ASAE*, vol. 28, no. 5, pp. 1673–1675, 1985, doi: 10.13031/2013.32497.

[18] O. Erkmen, “Modified-Atmosphere Storage of Foods,” in *Progress in Food Preservation*, Wiley, 2012, pp. 49–66. doi: 10.1002/9781119962045.ch3.

[19] R. Alimardani, M. Soltani, H. Mobli, and S. S. Mohtasebi, “Modified Atmosphere Packaging: A ProgressiveTechnology for Shelf-Life Extension of Fruits and Vegetables,” 2015, doi: 10.13140/RG.2.1.2822.0887.

[20] O. J. Caleb, P. V Mahajan, F. A.-J. Al-Said, and U. L. Opara, “Modified Atmosphere Packaging Technology of Fresh and Fresh-cut Produce and the Microbial Consequences—A Review,” *Food Bioprocess Technol.*, vol. 6, no. 2, pp. 303–329, 2013, doi: 10.1007/s11947-012-0932-4.

[21] J. M. DeLong, “Storage,” in *Encyclopedia of Applied Plant Sciences*, Elsevier, 2017, pp. 340–350. doi: 10.1016/B978-0-12-394807-6.00011-3.

[22] A. Paleczek, D. Grochala, and A. Rydosz, “Artificial Breath Classification Using XGBoost Algorithm for Diabetes Detection,” *Sensors*, vol. 21, no. 12, p. 4187, 2021,

doi: 10.3390/s21124187.

[23] B. Long, A. Koyfman, and M. A. Vivirito, “Capnography in the Emergency Department: A Review of Uses, Waveforms, and Limitations,” *J. Emerg. Med.*, vol. 53, no. 6, pp. 829–842, Dec. 2017, doi: 10.1016/j.jemermed.2017.08.026.

[24] D. R. Goldhill, T. M. Cook, and C. S. Waldmann, “Airway incidents in critical care, the NPSA, medical training and capnography,” *Anaesthesia*, vol. 64, no. 4, pp. 354–357, 2009, doi: 10.1111/j.1365-2044.2008.05856.x.

[25] J. L. Falk, E. C. Rackow, and M. H. Weil, “End-Tidal Carbon Dioxide Concentration during Cardiopulmonary Resuscitation,” *N. Engl. J. Med.*, vol. 318, no. 10, pp. 607–611, 1988, doi: 10.1056/NEJM198803103181005.

[26] E. Wollner *et al.*, “Impact of capnography on patient safety in high- and low-income settings: a scoping review,” *Br. J. Anaesth.*, vol. 125, no. 1, pp. e88–e103, Jul. 2020, doi: 10.1016/j.bja.2020.04.057.

[27] A. Webb, D. Angus, S. Finfer, L. Gattinoni, and M. Singer, Eds., *Oxford Textbook of Critical Care*, vol. 1. Oxford University Press, 2016. doi: 10.1093/med/9780199600830.001.0001.

[28] S. Verscheure, P. B. Massion, F. Verschuren, P. Damas, and S. Magder, “Volumetric capnography: lessons from the past and current clinical applications,” *Crit. Care*, vol. 20, no. 1, p. 184, Dec. 2016, doi: 10.1186/s13054-016-1377-3.

[29] Y. Colman and B. Krauss, “Microstream Capnography Technology: A New Approach to an Old Problem.,” *J. Clin. Monit. Comput.*, vol. 15, no. 6, pp. 403–409, 1999, doi: 10.1023/A:1009981115299.

[30] G. Yu, C. Liu, Y. Zheng, Y. Chen, D. Li, and W. Qin, “Meta-analysis in the production chain of aquaculture: A review,” *Inf. Process. Agric.*, May 2021, doi: 10.1016/j.inpa.2021.04.002.

[31] FAO, Ed., *Meeting the sustainable development goals*, no. 2018. Rome, 2018.

[32] S. Fivelstad, A. B. Olsen, H. Kløften, H. Ski, and S. Stefansson, “Effects of carbon dioxide on Atlantic salmon (Salmo salar L.) smolts at constant pH in bicarbonate rich freshwater,” *Aquaculture*, vol. 178, no. 1–2, pp. 171–187, 1999, doi: 10.1016/S0044-8486(99)00125-8.

[33] G. R. Smart, D. Knox, J. G. Harrison, J. A. Ralph, R. H. Richard, and C. B. Cowey, “Nephrocalcinosis in rainbow trout Salmo gairdneri Richardson; the effect of

exposure to elevated CO2 concentrations," *J. Fish Dis.*, vol. 2, no. 4, pp. 279–289, 1979, doi: 10.1111/j.1365-2761.1979.tb00170.x.

[34] S. Fivelstad, H. Haavik, G. Løvik, and A. B. Olsen, "Sublethal effects and safe levels of carbon dioxide in seawater for Atlantic salmon postsmolts: ion regulation and growth," *Aquaculture*, vol. 160, no. 3–4, pp. 305–316, 1998, doi: 10.1016/S0044-8486(97)00166-X.

[35] V. C. Mota *et al.*, "The effects of carbon dioxide on growth performance, welfare, and health of Atlantic salmon post-smolt (Salmo salar) in recirculating aquaculture systems," *Aquaculture*, vol. 498, pp. 578–586, 2019, doi: 10.1016/j.aquaculture.2018.08.075.

[36] T. Grandke and J. Hesse, "Introduction," in *Sensors*, Weinheim, Germany: Wiley-VCH Verlag GmbH, 2008, pp. 1–16.

[37] M. J. McGrath and C. N. Scanaill, "Sensing and Sensor Fundamentals," in *Sensor Technologies: Healthcare, Wellness, and Environmental Applications*, Berkeley, CA: Apress, 2013, pp. 15–50. doi: 10.1007/978-1-4302-6014-1_2.

[38] A. Dey, "Semiconductor metal oxide gas sensors: A review," *Mater. Sci. Eng. B*, vol. 229, pp. 206–217, 2018, doi: 10.1016/j.mseb.2017.12.036.

[39] M. Gardon and J. M. Guilemany, "A review on fabrication, sensing mechanisms and performance of metal oxide gas sensors," *J. Mater. Sci. Mater. Electron.*, vol. 24, no. 5, pp. 1410–1421, 2013, doi: 10.1007/s10854-012-0974-4.

[40] S.-W. Chiu and K.-T. Tang, "Towards a Chemiresistive Sensor-Integrated Electronic Nose: A Review," *Sensors*, vol. 13, no. 10, pp. 14214–14247, 2013, doi: 10.3390/s131014214.

[41] N. Barsan and U. Weimar, "Fundamentals of Metal Oxide Gas Sensors," in *Proceedings IMCS 2012*, 2012, pp. 618–621. doi: 10.5162/IMCS2012/7.3.3.

[42] Y. K. Gautam, K. Sharma, S. Tyagi, A. K. Ambedkar, M. Chaudhary, and B. Pal Singh, "Nanostructured metal oxide semiconductor-based sensors for greenhouse gas detection: progress and challenges," *R. Soc. Open Sci.*, vol. 8, no. 3, p. rsos.201324, 201324, 2021, doi: 10.1098/rsos.201324.

[43] H. Suzuki, H. Arakawa, S. Sasaki, and I. Karube, "Micromachined Severinghaus-Type Carbon Dioxide Electrode," *Anal. Chem.*, vol. 71, no. 9, pp. 1737–1743, 1999, doi: 10.1021/ac9811468.

[44] E. Dervieux, M. Théron, and W. Uhring, “Carbon Dioxide Sensing—Biomedical Applications to Human Subjects,” *Sensors*, vol. 22, no. 1, p. 188, 2021, doi: 10.3390/s22010188.

[45] S. Mulmi and V. Thangadurai, “Editors’ Choice—Review—Solid-State Electrochemical Carbon Dioxide Sensors: Fundamentals, Materials and Applications,” *J. Electrochem. Soc.*, vol. 167, no. 3, p. 037567, 2020, doi: 10.1149/1945-7111/ab67a9.

[46] A. Hulanicki, S. Glab, and F. Ingman, “Chemical sensors: definitions and classification,” *Pure Appl. Chem.*, vol. 63, no. 9, pp. 1247–1250, 1991, doi: 10.1351/pac199163091247.

[47] T.-V. Dinh, I.-Y. Choi, Y.-S. Son, and J.-C. Kim, “A review on non-dispersive infrared gas sensors: Improvement of sensor detection limit and interference correction,” *Sensors Actuators B Chem.*, vol. 231, pp. 529–538, Aug. 2016, doi: 10.1016/j.snb.2016.03.040.

[48] J. Kaur, V. Adamchuk, J. Whalen, and A. Ismail, “Development of an NDIR CO2 Sensor-Based System for Assessing Soil Toxicity Using Substrate-Induced Respiration,” *Sensors*, vol. 15, no. 3, pp. 4734–4748, Feb. 2015, doi: 10.3390/s150304734.

[49] D. Gibson and C. MacGregor, “A Novel Solid State Non-Dispersive Infrared CO2 Gas Sensor Compatible with Wireless and Portable Deployment,” *Sensors*, vol. 13, no. 6, pp. 7079–7103, 2013, doi: 10.3390/s130607079.

[50] D. F. Swinehart, “The Beer-Lambert Law,” *J. Chem. Educ.*, vol. 39, no. 7, p. 333, Jul. 1962, doi: 10.1021/ed039p333.

[51] J. M. Parnis and K. B. Oldham, “Beyond the Beer–Lambert law: The dependence of absorbance on time in photochemistry,” *J. Photochem. Photobiol. A Chem.*, vol. 267, pp. 6–10, 2013, doi: 10.1016/j.jphotochem.2013.06.006.

[52] T. R. Anderson, E. Hawkins, and P. D. Jones, “CO2, the greenhouse effect and global warming: from the pioneering work of Arrhenius and Callendar to today’s Earth System Models,” *Endeavour*, vol. 40, no. 3, pp. 178–187, 2016, doi: https://doi.org/10.1016/j.endeavour.2016.07.002.

[53] C. Driau, O. Casals, I. Benito-Altamirano, J. D. Prades, and C. Fàbrega, “Revisiting Colorimetric Gas Sensors: Compact, Versatile and Cost-Effective,” in *4th International Conference nanoFIS 2020 - Functional Integrated nanoSystems*,

2020, p. 20. doi: 10.3390/proceedings2020056020.

[54] A. Mills and K. Eaton, “Optical sensors for carbon dioxide: An overview of sensing strategies past and present,” *Quim. Anal.*, vol. 19, pp. 75–86, 2000.

[55] A. Mills, “Optical Sensors for Carbon Dioxide and Their Applications,” in *Sensors for Environment, Health and Security*, M.-I. Baraton, Ed. Dordrecht: Springer Netherlands, 2009, pp. 347–370. doi: 10.1007/978-1-4020-9009-7_23.

[56] J. P. Mendes *et al.*, “Dissolved Carbon Dioxide Sensing Platform for Freshwater and Saline Water Applications: Characterization and Validation in Aquaculture Environments,” *Sensors*, vol. 19, no. 24, p. 5513, 2019, doi: 10.3390/s19245513.

[57] J. Mendes, L. Coelho, C. M. De Melo Pereira, and P. Jorge, “Colorimetry-based System for Gaseous Carbon Dioxide Detection,” *U.Porto J. Eng.*, vol. 6, no. 2, pp. 59–69, 2020, doi: 10.24840/2183-6493_006.002_0006.

[58] A. Mills, Q. Chang, and N. McMurray, “Equilibrium studies on colorimetric plastic film sensors for carbon dioxide,” *Anal. Chem.*, vol. 64, no. 13, pp. 1383–1389, Jul. 1992, doi: 10.1021/ac00037a015.

[59] A. Mills and D. Yusufu, “Extruded colour-based plastic film for the measurement of dissolved CO2,” *Sensors Actuators B Chem.*, vol. 237, pp. 1076–1084, Dec. 2016, doi: 10.1016/j.snb.2016.07.141.

[60] “Hamamatsu, RGB color sensor, S9032-02 datasheet, May 4 2022.” 2022.

[61] A. Campilho, *Instrumentação electrónica: métodos e técnicas de medição*. FEUP edições, 2000.

[62] C. Neff, M. Trapuzzano, and N. B. Crane, “Impact of vapor polishing on surface quality and mechanical properties of extruded ABS,” *Rapid Prototyp. J.*, vol. 24, no. 2, pp. 501–508, Mar. 2018, doi: 10.1108/RPJ-03-2017-0039.

Appendix A

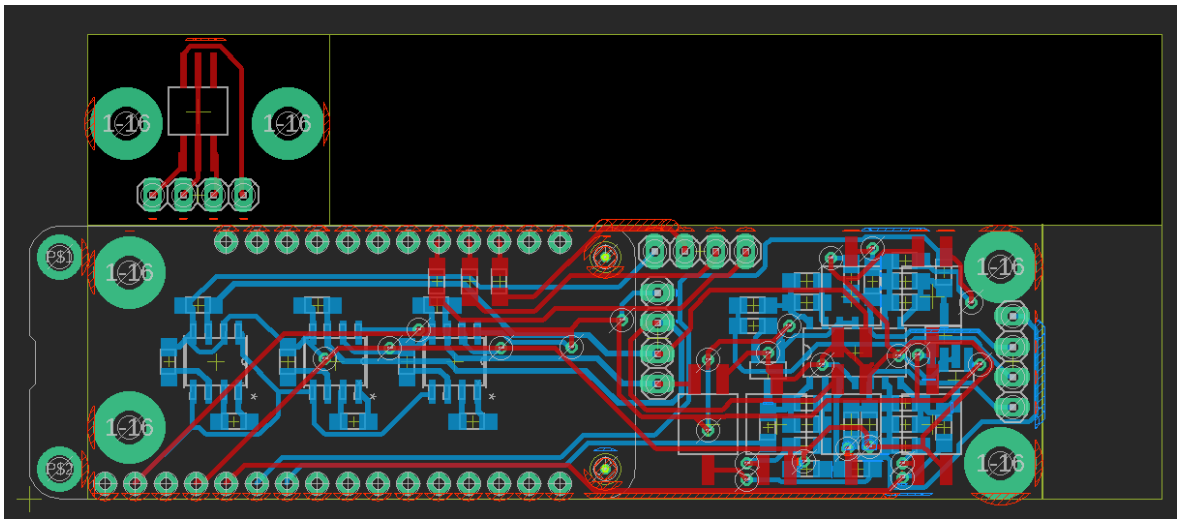

Figure A.1: Printed circuit board of the amplification circuit.

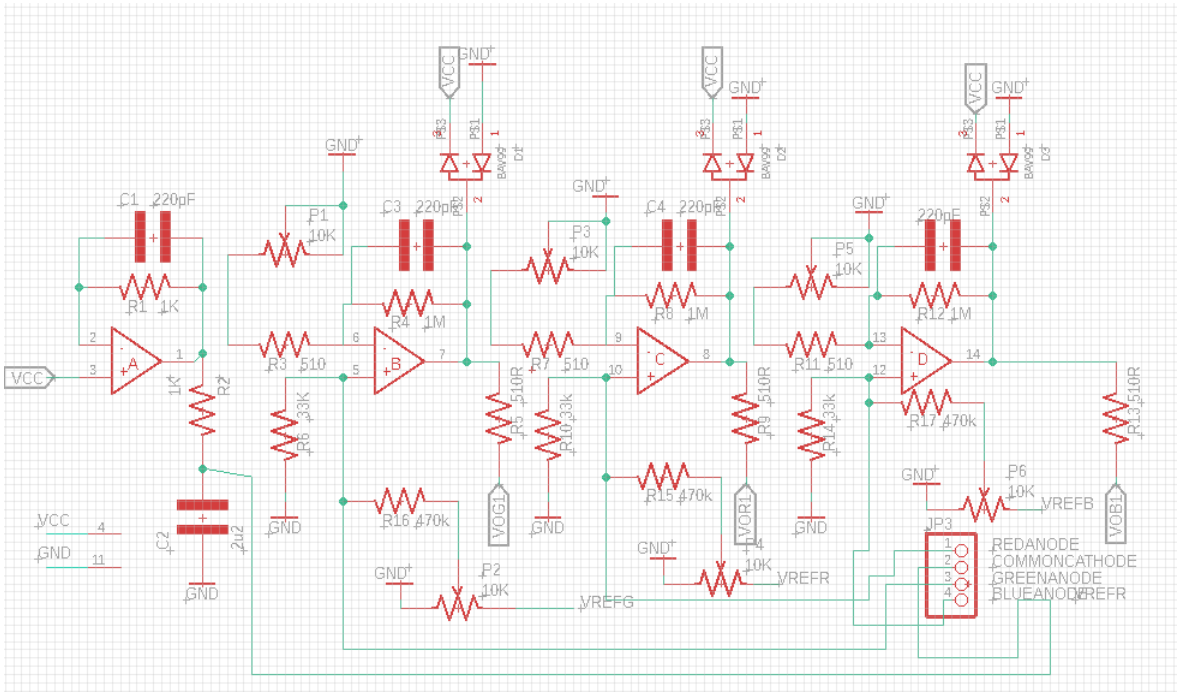

Figure A.2: Schematic of the amplification circuit.